I&EC research
Industrial & Engineering Chemistry Research

pubs.acs.org/IECR

Article

Model Development, Validation, and Optimization of an MEA-Based Post-Combustion CO_2 Capture Process under Part-Load and Variable Capture Operations

Paul Akula, John Eslick, Debangsu Bhattacharyya,* and David C. Miller

Cite This: https://doi.org/10.1021/acs.iecr.0c05035

Read Online

ACCESS | Metrics & More | Article Recommendations | Supporting Information

ABSTRACT: Existing power plants are frequently load-following due to increasing penetration of the renewables into the grid. For power plants integrated with CO_2 capture, optimal operation of the capture unit at part-load and variable capture conditions can be exploited to reduce the operating costs. This paper presents insights into the performance of a reference monoethanolamine (MEA)-based post-combustion CO_2 capture unit under steady-state part-load and variable capture operations. A rigorous plant-wide model for the capture unit is developed in the Institute for Design of Advanced Energy Systems computational platform. The contactor model is validated with the data from a wetted wall column (WWC) and two pilot plants. The plant-wide model is used for steady-state optimization under part-load operations and variable capture rates using flue gas similar to pulverized coal and natural gas-combined cycle power plants. Analysis on the performance of the reference rich/lean amine heat exchanger shows that the hot-end temperature approach can considerably vary under part-load operations for a given heat exchanger area. The study shows that if the plant is not optimally operated under part-load and variable capture operations, there can be a high penalty depending on the deviation of the liquid/gas flowrate with respect to its optimal value. This study shows that the optimal operation of an existing capture unit is crucial for minimizing the energy penalty under part-load and variable capture operations.

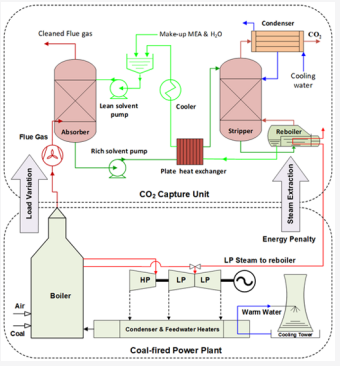

1. INTRODUCTION

Post-combustion CO_2 capture (PCC) can considerably reduce the amount of CO_2 emitted from industrial sources. PCC using amines is the most commercially mature technology for retrofitting the existing power stations.[1−5] However, integration of the amine-based capture plant with power plants incurs an energy penalty resulting in as high as a 22.9% point decrease in the power plant efficiency.[6,7] As power plants cycle more due to increased penetration of renewables into the grid,[8−11] the downstream capture plant will face considerable disturbances due to rapid and large changes in the flue gas flowrate and CO_2 concentration.[12−14] He et al.[14] observed that as the flue gas load varies at high frequency, it can have a large impact on the CO_2 capture rate. Mac Dowell and Shah[15] presented a multiperiod optimization framework that decouples the operation of the power plant from the efficiency penalty imposed by the capture plant. Six distinct operating periods due to electricity price variation in a day were identified. It was observed that the power plant operated relatively steadily for longer hours at a given load factor.

While many of the papers referenced before are focused on the dynamic operation of the capture plant, the capture plant can also operate at steady state under part-load and variable capture conditions. Thus, steady-state optimization can be helpful for improving the economics of the capture plant. This work is focused on developing a predictive, steady-state model and using it for optimization of part-load and variable capture operations. The literature review provided below mainly reviews the existing literature from the steady-state perspective with references to some papers that have evaluated the dynamic performance as relevant for the discussion. Sections 1.1, 1.2, and 1.3 review the existing literature on model complexity, model validation, and optimization, respectively.

1.1. Model Complexity for Part-Load and Variable Capture Studies.

Many research studies have focused on developing detailed process models of CO_2 capture plants, with emphasis on the absorber and stripper.[13,16,17] In addition to differences in the properties and reaction kinetic models in these studies, these models greatly differ in how mass transfer and heat transfer resistances are represented. While the nonequilibrium stage model[18−20] that considers spatial variation in mass transfer and heat transfer fluxes in the films along with chemical reactions[21−23] can be very

Received: October 14, 2020
Revised: March 10, 2021
Accepted: March 11, 2021

accurate, these models can be computationally challenging for plant-wide optimization. Another approach that provides a compromise between computational tractability and accuracy is to model the mass transfer resistance in the gas and liquid films by considering a linear driving force between the interface of the films and bulk gas and liquid phases, respectively, where the mass transfer enhancement due to chemical reactions is captured by using an enhancement factor.[24] Many authors have used the enhancement factor-based model for optimization and control applications.[14,25−27] Patron and Ricardez-Sandoval[25] used an enhancement factor-based model to design a robust nonlinear model-predictive controller. The authors noted that an accurate model of the plant is necessary for obtaining good control performance. Typically, pseudo-first-order and instantaneous reversible reactions are assumed for computing the enhancement factors for absorption and stripping, respectively.[28−33] However, these assumptions may not adequately represent all of the reaction regimes occurring along the packing height during widely variable absorption and stripping conditions[34] expected for part-load and variable capture operations of the CO_2 capture unit. Dang and Rochelle[35] have shown that a more accurate enhancement factor model is required at high loading. Commonly used enhancement factor models are those developed by van Krevelen and Hoftijzer[36] and Savage et al.[37] The enhancement factor model developed by van Krevelen and Hoftijzer is given by an implicit equation based on the assumption that the concentration of the dissolved unreacted gas in the liquid bulk is zero. Under these assumptions, the enhancement factor can be explicitly calculated.[38−41] Savage et al.[37] improved the model of van Krevelen and Hoftijzer to account for reversible and instantaneous reaction regimes. Gaspar et al.[34] have presented a general method (GM) for calculating the enhancement factor that is superior to the aforementioned methods and can adequately account for the instantaneous, fast, and intermediate reaction regimes over wide temperature and loading ranges; however, the enhancement factor can no longer be calculated explicitly, instead requiring the solution of a system of nonlinear equations. Gaspar et al.[34] have recommended the secant method for obtaining the enhancement factor using the GM. In this work, we show that, with appropriate bounds on the enhancement factor and a step-by-step initialization routine developed using the Institute for Design of Advanced Energy Systems (IDAES) Process Systems Engineering (PSE) computational platform,[42] the GM can be solved reliably for tower design and optimization under widely varying process conditions. The IDAES platform is built on Pyomo, an algebraic modeling language,[43] with interfaces to several optimization algorithms such as IPOPT.[44] More details on IDAES can be found later in this paper and at https://github.com/IDAES.

For minimizing the energy penalty of the capture plant, the balance of plant (BOP), especially the rich/lean solvent heat exchanger (RL-HX) and the reboiler, plays a key role. Although little attention is typically given to the rich/lean solvent heat exchange in most papers, the heat exchanger type and design are crucial in minimizing the energy penalty associated with amine-based CO_2 capture process[45,46] and is even more significant under part-load and variable capture operations of the CO_2 capture unit. Several authors have modeled the RL-HX by fixing the hot-end temperature approach for optimization studies.[47−50] However, fixing the temperature approach of the heat exchanger may not be suitable for capturing the energy interactions under part-load operations. The RL-HX is often modeled as a countercurrent shell and tube heat exchanger;[29,51,52] however, in pilot plant operations, a plate heat exchanger (PHE) is used for rich/lean solvent heat exchange since the PHE offers low-temperature approach compared to the conventional shell and tube exchangers,[53] thus helping to reduce the energy penalty. Lin and Rochelle[46] developed a model of a PHE to minimize the cost of the exchanger by considering the fluid velocity and log mean temperature difference (LMTD) as the decision variables. Authors of this paper previously presented validation studies of a RL-HX model using pilot plant data. In this work, a rigorous algebraic model of a PHE based on the effectiveness-number of transfer unit (ε-NTU) approach is developed and validated with pilot plant data, and used for plant-wide optimization studies.[45]

More attention has been given to the reboiler unit compared to that of the RL-HX as the energy penalty associated with the amine plant stems primarily from steam consumption in the reboiler.[47,49,54] However, a simple heat exchanger model is typically used[29,31,51] based on the mass and energy balances along with the vapor−liquid equilibrium (VLE) for calculating the steam consumption in the reboiler. A model that includes mass and energy balances along with the consideration of physical and chemical equilibria by taking into account the speciation model[55] is desired. Arce et al.[56] used the statistical associating fluid theory (SAFT) thermodynamic model[57] incorporating the effect of reactions in their thermodynamic model. In this paper, a reboiler model that includes the speciation model in the liquid phase is presented and validated together with the generalized column model for various stripper operating conditions.

1.2. Model Validation. Models intended for optimization under part-load and variable capture conditions should be validated using data from multiple scales and from broad operating conditions as would be expected under off-design conditions.[58−61] Most often, models are validated using data from only one scale, i.e., either from the laboratory or from the pilot plant scale, but not both. Data from the pilot plant at the University of Texas, Austin,[62,63] that includes two identical columns (6.1 m height, 0.427 m internal diameter) have been used by various authors.[29,33,52,64,65] Those data include the effect of variations in solvent and gas flowrates, lean CO_2 loading, stripper pressure, and packing type. Llano-Restrepo and Araujo-Lopez[17] validated their absorber model using the data presented by Sønderby et al.[66] from a pilot absorber (0.1 m internal diameter and 1.6−8.2 m variable height) for variable solvent flowrate and CO_2 loading. Tobiesen et al.[32,67] presented data from a facility with an absorber (0.15 m internal diameter and 4.36 m height) and desorber (0.1 m internal diameter and 4.1 m height) and a capture capacity of about 10 kg CO_2/h and a reboiler with an 18 kW maximum capacity. These data have been used by various researchers[28,56] to validate the columns over a range of process conditions. Bui et al.[68] used the data from the U.K. Carbon Capture and Storage Research Center (UKCCSRC) Pilot-scale Advanced Capture Technology (PACT) pilot plant to validate their models of the absorber (6.5 m high and 0.3 internal diameter) and stripper columns (6.1 m high and 0.3 internal diameter). In a recent study, Bui et al.[69] used data from the world's largest test facility for carbon capture technologies (Norway's Technology Centre

https://doi.org/10.1021/acs.iecr.0c05035
Ind. Eng. Chem. Res. XXXX, XXX, XXX−XXX

Mongstad, TCM) to validate their model. Pilot plant test runs are costly and time consuming;[70] therefore, the collection of large amounts of data from pilot plants can be challenging. Additional data collected from bench-scale experiments, such as a wetted wall column (WWC) that has well-quantified contact area,[71−75] can be very useful not only because large amounts of data covering wide operating regimes can be collected from these lab-scale devices using considerably less resources but also due to lower uncertainty in the data. Data from both pilot plants and WWCs can be utilized to validate models under widely different operating conditions.[55,58,76−79] In this work, the generic contactor model and the plate heat exchanger model are validated using data from the National Carbon Capture Center (NCCC) located in Wilsonville, Alabama, under considerable variation of the solvent flowrate, gas flowrate, CO_2 concentration in the gas, and reboiler steam flowrate as would be expected under the part-load operation of the host power plant. The same contactor model was modified to represent the WWC and validated using data from Dugas.[75] In addition, the absorber and stripper contactor columns are scaled up and validated with the TCM pilot data.[80]

1.3. Optimal Operating Conditions under Part-Load and Variable Capture Conditions. Capital and operating costs (OPCs) of capture plants strongly depend on the configuration.[12,81−83] For a given configuration, operating conditions play a vital role in reducing the operating costs. Optimal operating conditions can greatly vary under part-load and variable capture operations of the capture plant depending on the plant configuration and operational strategies. Various operating strategies have been proposed for off-design operations including flue gas venting or bypassing, solvent storage, and degree of solvent regeneration.[15,69,82,84−91] Under the flue gas venting/bypassing option, the CO_2 capture plant may vent/bypass the flue gas completely or partially. Under the solvent storage option, CO_2 capture is accomplished by feeding the absorber from a lean solvent storage tank while storing the resulting rich solvent in another tank to be regenerated later, thus saving steam consumption in the reboiler. The stored rich solvent is regenerated during periods of low electricity demand. This strategy maximizes the net electricity available for export during high demand while maintaining the CO_2 removal target, but additional cost is incurred for solvent inventory, storage tanks, and larger process equipment items. If the degree of solvent regeneration is varied under off-design operation in response to electricity demand, the CO_2 removal target also varies as the reboiler steam rate is adjusted. Ziaii et al.[49] observed that a 10% reduction in the reboiler duty decreased the CO_2 removal target from 90 to 81% with adjustment of the rich solvent flowrate to the stripper to maintain a constant lean load leaving the stripper and 80.3% without the adjustment. In a later contribution, Ziaii et al.[90] noted that while flue gas venting is a similar strategy, better process control can be achieved by varying the degree of solvent regeneration to keep the capture unit close to the optimal conditions under part-load operations. Bui et al.[69] demonstrated the time-varying solvent regeneration strategy on a large-scale CO_2 capture pilot plant.[92] For the transition from "peak" to "off-peak" period of electricity demand, the lean loading (mol/mol) was observed to decrease from 0.48 to 0.16 and the CO_2 capture rate increases from 14.5 up to 89−97%. Another strategy is to capture a lower amount of CO_2 without bypassing the flue gas. Compared to bypassing/venting the flue gas, this strategy has the advantage that the absorber operates under higher CO_2 partial pressures when a lower amount of CO_2 is captured, thus reducing the energy penalty. In this paper, variable capture rates are evaluated at a target removal rate of 75−90% by an increment of 5% without considering the transient response. Hence, a steady-state plant-wide optimization is conducted to determine the optimum conditions under part-load operations and variable capture rates.

The optimum conditions also vary considerably depending on the flue gas flowrate and/or inlet flue gas CO_2 composition (e.g., depending on whether the flue gas is sourced from a natural gas-combined cycle power plant or a coal-fired power plant). Studies considering the effect of flue gas CO_2 composition on amine-based CO_2 capture systems have been conducted by various authors.[47,48,93−100] Mores et al.[101] developed a mathematical model for amine-based post-combustion CO_2 capture and formulated an optimization problem in the general algebraic modeling system (GAMS) platform to minimize the total annual cost via simultaneous optimization of the operating conditions (solvent flowrates, temperatures, and pressures) and dimensions of the equipment (absorbers, strippers, heat exchangers, pumps, and compressors); however, the column model was simplified to use the Murphree efficiency to capture mass transfer limitations. The optimization was repeated for several CO_2 removal targets (70−95%) for a fixed flue gas flowrate (10 kmol/s) and CO_2 composition (4.22%). Hasan et al.[97] used the RADFRAC model in Aspen Plus to minimize the total annualized cost of the CO_2 capture process. The optimization was performed for different flue gas flowrates (0.1−10 kmol/s) and CO_2 compositions (1−70 vol %) to capture at least 90% of CO_2. Oh and Kim[102] developed an equilibrium-based model for an monoethanolamine (MEA) solvent in UniSim. They minimized the energy requirement for different part-load operations to maintain a 90% capture rate; however, rate-based models for reactive absorption are preferable for optimization studies to take into account mass transfer limitations.[18,103,104] Choi et al.[105] used Unisim interfaced with Matlab for modeling the CO_2 capture unit and optimizing it for flue gases from nonpower industries representing a variation in flue gas flowrate and CO_2 content. Feron et al.[98] recently presented a study on the technoeconomic performance for CO_2 capture above 90% from a natural gas-combined cycle plant and a coal-fired power plant. The model was developed using ProTreat considering a fixed temperature approach of 20 °C in the rich−lean cross heat exchanger. The review of the literature on the plant-wide optimization of CO_2 capture plants presented above identifies the following limitations that this work seeks to address: (i) CO_2 removal rate is set at 90% or varied within a narrow range, while the capture rate is expected to vary considerably under variable capture scenario while achieving a cumulative target capture over a period of time, (ii) simultaneous variation of the flue gas flowrate, composition, and capture is typically not considered; however, under part-load and variable capture operations, it is likely that the power plant is load-following; thus, both the flowrate and composition of the flue gas are likely to vary depending on the technology of the power plant, its design, fuel composition, operational strategy, etc., (iii) several part-load optimization studies consider a fixed temperature approach in the lean/rich heat

https://doi.org/10.1021/acs.iecr.0c05035
Ind. Eng. Chem. Res. XXXX, XXX, XXX−XXX

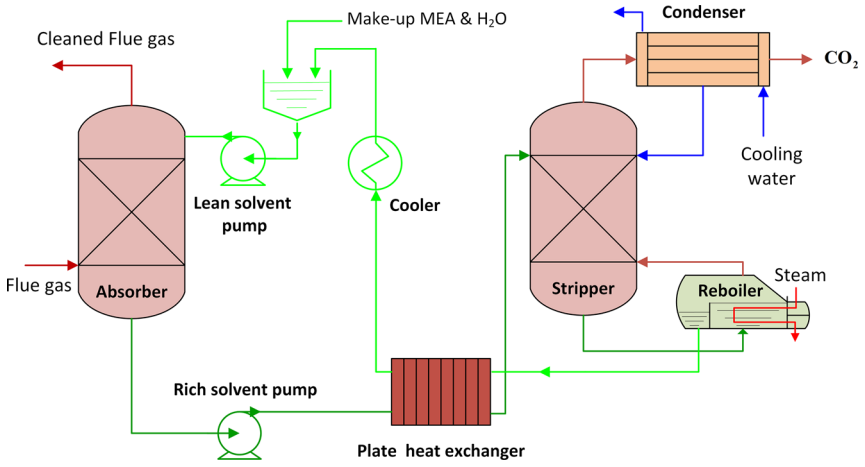

Figure 1. Amine plant for the CO_2 capture process.

exchanger, but the temperature approach is likely to vary under off-design operations when using an existing heat exchanger due to the fixed heat transfer area.

This paper focuses on plant-wide model development, validation with multiscale data, and mathematical optimization for variable capture under steady-state part-load operations. In particular, the main contributions of this work are as follows:

(a) A generic rate-based packed column model is developed and validated using the WWC data and data from NCCC and TCM pilot plants. The contactor model uses an enhancement factor model that is superior to the Hatta number approximation and more accurate for a wide range of operating conditions.
(b) The PHE model is validated with the pilot plant data and used for simulation and optimization of the plant-wide model.
(c) The model is implemented in the IDAES framework with a four-level initialization strategy that aids in convergence while simulating part-load and variable capture operations. The framework readily facilitates equation-oriented, simultaneous optimization of the plant-wide model using advanced optimization solvers.
(d) The impact of temperature approach in the rich−lean heat exchanger on the energy penalty under steady-state part-load operations is accounted for by using a rigorous plate heat exchanger model that is validated using the pilot plant data.
(e) Steady-state optimization under part-load and variable capture operations is performed considering high and low flue gas compositions that are similar to those from the pulverized coal and NGCC power plants, respectively.

The rest of the paper is organized as follows: Section 2 describes the mathematical model of the process units for the amine plant CO_2 capture. Model implementation and validation are presented in Section 3, while the results and off-design optimization studies are presented in Section 4. The summary of findings and future remarks are given in Section 5. For brevity, the process model equations, property models, and reconstitution of apparent species from true species[106] are presented in the Supporting Information document along with the data from NCCC and TCM for steady-state validation.

2. MODEL DEVELOPMENT OF AMINE CO_2 CAPTURE PROCESS

A typical amine-based CO_2 capture plant is shown in Figure 1. In the absorber, CO_2 is absorbed from the flue gas into the lean amine solution. The rich amine solution leaving the bottom of the absorber is preheated in a rich/lean amine heat exchanger and sent to the stripper to desorb the dissolved CO_2. Low-pressure (LP) steam extracted from the steam turbine of the power plant is typically used in the reboiler of the stripper. The hot lean solvent leaving the stripper is recycled back to the absorber after being cooled in the rich/lean crossover heat exchanger followed by a water cooler. The mathematical models of the main process units are described in Section 2.1, while the detailed equations are provided in the Supporting Information. The required property models of the CO_2−MEA−H_2O system are described in Section 2.2 and in more detail in the Supporting Information.

2.1. Model Description. Considering the packed columns, reactive absorption and desorption processes are more adequately described by rate-based (nonequilibrium) models than traditional equilibrium models.[104] In this work, a generic rate-based model is developed for simulation of both absorber and stripper columns under the assumption of plug flow, which is expected to be satisfactory at low pressure and liquid/gas velocities less than 3 m/s.[67] Model equations can be found in the Supporting Information. The rate-based column model consists of molar component balances, enthalpy balances, heat and mass transfer rate equations (eqs S1−S13), speciation model in the liquid phase due to reactions, and enhancement factor model. The vapor-side interface composition of CO_2 is calculated by using the continuity of fluxes and existence of phase equilibrium at the interface.

The speciation model in the liquid phase due to reactions and the enhancement factor model are critical to the evaluation of the column models. The aqueous-phase chemical reactions for the CO_2−MEA−H_2O system are modeled with the following reversible reactions from the literature.[107,108] Morgan et al.[108] have noted that the two reactions in eqs 1 and 2 represent the chemistry of the CO_2-loaded monoethanolamine solution adequately

$$2\mathrm{MEA} + \mathrm{CO_2} \rightleftarrows \mathrm{MEAH^+} + \mathrm{MEACOO^-} \quad (1)$$

https://doi.org/10.1021/acs.iecr.0c05035
Ind. Eng. Chem. Res. XXXX, XXX, XXX−XXX

$$MEA + CO_2 + H_2O \rightleftarrows MEAH^+ + HCO_3^- \quad (2)$$

Reaction kinetics are included in the liquid film model, while chemical equilibrium is assumed to prevail in the bulk liquid. The speciation model comprises eqs 3−8 that determine the distribution of the true species in the bulk liquid. Equations 3 and 4 are the concentration-based equilibrium expressions, while the material balances are given in eqs 5−8. A systematic approach is used for deriving the material balances via reconstitution of apparent species from true species[106] and is described in the Supporting Information. Equation 5 is the MEA balance, eq 6 is the CO_2 balance, eq 7 is the water balance, and eq 8 is the electroneutrality condition for charged species in the liquid phase. C_i^t is the true species concentration of the species in the liquid phase

$$K_1 = \frac{C^t_{MEACOO^-,L} C^t_{MEAH^+,L}}{C^t_{CO_2,L} (C^t_{MEA,L})^2} \quad (3)$$

$$K_2 = \frac{C^t_{MEAH^+,L} C^t_{HCO_3^-,L}}{C^t_{CO_2,L} C^t_{MEA,L} C^t_{H_2O,L}} \quad (4)$$

$$C^t_{MEA,L} + C^t_{MEACOO^-,L} + C^t_{MEAH^+,L} = C^a_{MEA,L} \quad (5)$$

$$C^t_{CO_2,L} + C^t_{MEAH^+,L} = C^a_{CO_2,L} \quad (6)$$

$$C^t_{H_2O,L} + C^t_{MEAH^+,L} - C^t_{MEACOO^-,L} = C^a_{H_2O,L} \quad (7)$$

$$C^t_{MEAH^+,L} = C^t_{HCO_3^-,L} + C^t_{MEACOO^-,L} \quad (8)$$

A computationally efficient approximate method to capture the effect of reaction on the mass transfer rate is to use the enhancement factor. While use of this approach helps to reduce the computational cost, typical enhancement factor approximations[37,109] are restricted to a given reaction regime. Gaspar et al.[34] have presented a general method (GM) for calculating the enhancement factor for all reaction regimes for reversible reactions under absorption and desorption conditions. In their approach,[34] the set of differential equations describing mass transport in the liquid film is transformed into a set of algebraic equations, as shown in eqs 9−16. E and $\Upsilon_{MEA}{}^i$ are the two unknowns in eqs 9 and 10. $\gamma^i_{MEAH^+}$, $\gamma^i_{MEACOO^-}$, and $\gamma^*_{CO_2}$ are the dimensionless concentrations of the reaction products, which depend on $\gamma_{MEA}{}^i$ (dimensionless concentration of MEA at the interface), as given in eqs 11−13. E^*_∞ is the instantaneous enhancement factor. $\gamma^b_{CO_2}$ is a dimensionless concentration driving force, where for $\gamma^b_{CO_2} < 1$, absorption occurs and for $\gamma^b_{CO_2} > 1$, desorption occurs. k_{rx} is the overall reaction rate constant of CO_2, while Ha is the Hatta number. $D_{i,L}$ is the diffusivities of the species in the solvent

$$E = 1 + (E^*_\infty - 1)\frac{(1 - \Upsilon^i_{MEA})}{(1 - \Upsilon^b_{CO_2})} \quad (9)$$

$$E = Ha\sqrt{\Upsilon^i_{MEA}}\,\frac{1 - \Upsilon^*_{CO_2}}{1 - \Upsilon^b_{CO_2}} \quad (10)$$

$$\Upsilon^*_{CO_2} = \Upsilon^b_{CO_2}\Upsilon^i_{MEAH^+}\Upsilon^i_{MEACOO^-}(\Upsilon^i_{MEA})^{-2} \quad (11)$$

$$\Upsilon^i_{MEAH^+} = 1 + \frac{D_{MEAH^+,L} C^t_{MEA}}{2D_{MEAH^+,L} C^t_{MEAH^+}}(1 - \Upsilon^i_{MEA}) \quad (12)$$

$$\Upsilon^i_{MEACOO^-} = 1 + \frac{D_{MEA,L} C^t_{MEA}}{2D_{MEACOO^-,L} C^t_{MEACOO^-}}(1 - \Upsilon^i_{MEA}) \quad (13)$$

$$E^*_\infty = 1 + \frac{D_{MEA,L} C^t_{MEA}}{2D_{CO_2,L} C^*_{CO_2}} \quad (14)$$

$$\Upsilon^b_{CO_2} = \frac{C^t_{CO_2}}{C^*_{CO_2}} \quad (15)$$

$$Ha = \frac{(k_{rx} C^t_{MEA} D_{CO_2,L})^{0.5}}{k_{L,CO_2}} \quad (16)$$

In addition to the generic column model, a model of the WWC is also developed. WWC is very useful for studying kinetic and mass transfer characteristics of reactive gas−liquid systems since it has a well-defined gas−liquid interfacial area. In this work, the generic packed column model is modified into a WWC model by considering the volume of the column based on the volume of the WWC annular space. The WWC model comprises the same equations as the tower model except that the packing characteristics such as the interfacial area and hydraulic diameter are removed while calculating those parameters based on the dimensions of the WWC.

Another key process unit is the rich−lean cross heat exchanger (RL-HX), which preheats the rich solvent leaving the absorber to reduce the reboiler and cooling duties required for amine-based PCC processes. In this work, the RL-HX model is developed as a plate heat exchanger (PHE) model as typically found in pilot plants. The authors[45] previously presented a rigorous model of a PHE using the effectiveness-number of transfer unit (ε-NTU) approach, which is adopted in this work. A summary of the equations can be found in the Supporting Information, while more details can be found in our earlier publication.[45]

The stripper reboiler is the major energy-consuming unit. The reboiler is developed as a single-stage equilibrium model at steady state, as described by eqs S14−S18 in the Supporting Information. The expressions for the chemical equilibrium, material balance for the true species, and the phase equilibrium constraints, which govern the distribution of the components between the vapor and liquid phases, are the same as those for the tower models given by eqs 3−8, S9, and S10. The condenser is also developed as an equilibrium stage model with a vapor inlet, a vapor outlet, and a liquid outlet, as described by eqs S19−S21. As shown in Figure 1, other process units include the cooler, which cools the lean solvent before entering the absorber and the mixing tank that combines the cool lean solvent with makeup MEA and water.

2.2. Properties of the CO_2−MEA−H_2O Capture System. The accuracy of the process models is strongly dependent on the quality of the underlying submodels. These submodels include property models and correlations such as physical properties (thermodynamic and transport properties), reaction kinetics, correlations for mass and heat transfer coefficients, and column hydraulics. The thermodynamic properties for both the liquid and vapor phases are summarized in Table 1, while the transport properties for

https://doi.org/10.1021/acs.iecr.0c05035
Ind. Eng. Chem. Res. XXXX, XXX, XXX−XXX

Table 1. Thermodynamic Properties

property	reference/remark
liquid density and molar volume	Morgan et al.[110]
vapor density and molar volume	ideal gas
specific heat capacity of liquid (MEA, H_2O)	Hilliard[107]
specific heat capacity of the CO_2-loaded solution	Agbonghae et al.[111]
vapor heat capacity	Smith[112]
heat of H_2O vaporization	Que and Chen[113]
heat of CO_2 absorption	Kohl and co-authors[114,115]
activity coefficient	parameters from Morgan et al.[108]
Henry's constant	Jiru et al.,[116] Morgan et al.[108]
H_2O vapor pressure	Smith[112]
concentration-based equilibrium constants	parameters regressed by Morgan et al.[108]

the rate-based model are summarized in Table 2 and the correlations for mass and heat transfer coefficients and

Table 2. Transport Properties

property/correlation	reference/remark
viscosity of the liquid solution	Morgan et al.[110]
viscosity of the vapor components	Sutherland[118]
vapor viscosity	Sutherland,[118] Wilke[119]
liquid thermal conductivity	Sato–Riedel correlation,[120] Li's mixing rule[121]
vapor thermal conductivity	Reid et al.[120]
binary diffusivity of vapor components	Seader and Henly,[122] Fuller correlation
diffusivity of CO_2 in aqueous MEA	Ying and Eimer[117,123]
diffusivity of MEA in solution	Snijder et al.[124]
diffusivity of $MEAH^+$ and $MEACOO^-$	Hoff et al.[125]
liquid surface tension	Asprion,[126] Morgan et al.[110]

Table 3. Correlations for Transfer Rates, Kinetic, and Column Hydraulics

property/correlation	reference/remark
second-order rate constant	Luo et al.[73]
convective heat transfer coefficients	Chilton–Colburn analogy
vapor and liquid mass transfer coefficients	Billet and Schultes,[127] Soares Chinen et al.[58]
interfacial area	Tsai et al.[128] Soares Chinen et al.[58]

column hydraulics are given in Table 3. Details of the various property models are in eqs S22–S49 in the Supporting Information.

3. MODEL IMPLEMENTATION AND VALIDATION

The implementation of the unit models in IDAES is shown in Section 3.1, and the approach to model validation and the numerical scheme for initialization are shown in Sections 3.2 and 3.3, respectively.

3.1. Model Implementation in IDAES Framework. The IDAES computational platform was used for this work.[42] IDAES is based on the Pyomo modeling and optimization language and supports rigorous large-scale process optimization. The IDAES platform provides basic modular flowsheeting features with full derivative information that permits the use of state-of-the-art optimization solvers. In this work, the unit process models including all property submodels are implemented in a common simulation environment, where all variables and parameters are easily accessible. In particular, the flowsheet for the CO_2 capture process is developed using the general column unit model for absorption/stripping and other unit models such as PHE, kettle reboiler, and partial condenser. Figure 2 shows the implementation of a packed

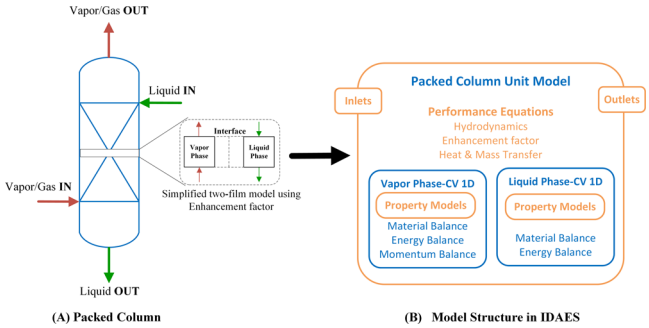

Figure 2. Unit model implementation in the IDAES framework using the control volume 1 dimension (CV 1D) block.

column unit model using the enhancement factor approach to describe heat and mass transfer across the interface as a continuous differential contactor (CDC) model. The CDC model has blocks for property submodels, inlet and outlet ports, and control volume (denoted as the holdup block in IDAES), where the performance equations for the vapor and liquid phases are included.

3.2. Experimental Data for Validation. For model validation, data from the WWC at the University of Texas, Austin,[75] are used along with the data from the National Carbon Capture Center (NCCC) pilot plant. In addition, the absorber and stripper columns are validated with the TCM pilot plant data[80] shown in Tables S20 and S21 in the Supporting Information. The WWC at the University of Texas, Austin, consists of a metal cylinder of 1.26 cm outside diameter and a length of 9.1 cm. The interfacial area is 38.52 cm^2, with a specific interfacial area (a_e) of 110.79 m^2/m^3 and a hydraulic diameter of 1.28 cm. The metal cylinder is enclosed in a glass tube of 2.54 cm outside diameter. The reaction zone is enclosed in a heat bath made from a 10.16 cm outside diameter glass tube. A large amount of data from this system is available[75] and is used to validate the WWC model.

The pilot solvent test unit (PSTU) at the NCCC as described in Morgan et al.[55] has a CO_2 capture capacity of 10 tons/day. The configuration of the NCCC absorber, stripper, and PHE is shown in Figure 3. The equipment sizes and dimensions for the NCCC process units are shown in Table 4. The absorber has two intercoolers that can remain online or offline, as desired. The data for the NCCC process units are shown in Tables S17–S19 in the Supporting Information.

3.3. Initialization Strategy. The general column model is a 1D rate-based model consisting of differential and algebraic equations (DAE) and is solved in IDAES using the interior point algorithm, IPOPT.[44] The packed bed model was discretized using the Pyomo DAE finite difference method with 20 finite elements resulting in 939 constraints and 7053 expressions. For aiding in convergence, especially in the absence of a "good" initial guess, an initialization routine is developed. Two homotopy/continuation parameters (λ_1,λ_2)

https://doi.org/10.1021/acs.iecr.0c05035
Ind. Eng. Chem. Res. XXXX, XXX, XXX–XXX

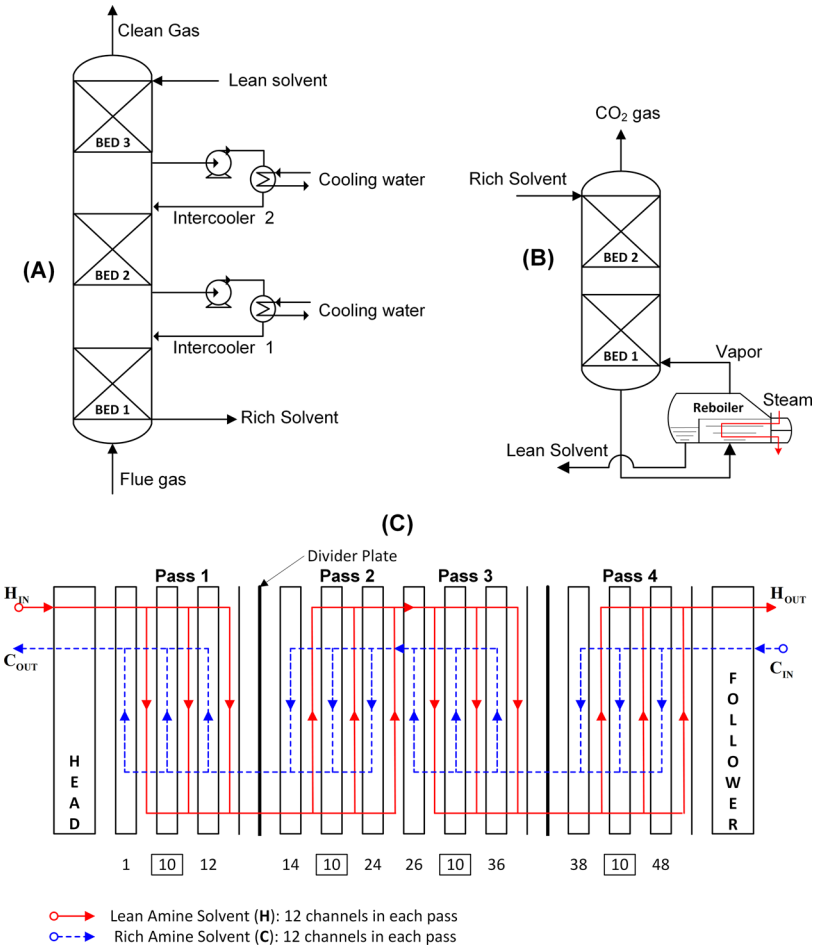

Figure 3. Configuration of NCCC unit models: (a) absorber with intercoolers, (b) stripper and reboiler, and (c) PHE.

Table 4. NCCC Design Parameters for Unit Model Validation

parameter	value
absorber/stripper diameter (m)	0.64/0.59
absorber/stripper bed height (m)	6.096/6.096
absorber/stripper no. of beds	3/2
absorber/stripper packing type	MellapakPlus 252Y
PHE plate length/width (m)	1.657/0.849
PHE plate thickness/gap (m)	0.0006/0.0038
PHE no. of passes/channels per pass	4/12
PHE port diameter (m)	0.3

are employed for the initialization procedure, as shown in Figure 4. The functions, $(g_1(X), g_2(X), f(X))$, describe the model equations when the homotopy parameters become zero or unity. The initialization routine for each packed bed in the column first solves only mass balance equations by turning off the heat and mass transfer rate equations. Then, the isothermal chemical absorption continuation parameter, λ_2, is used to turn on the mass transfer equations gradually with values ranging from 0 to 1. Subsequently, the adiabatic chemical absorption continuation parameter λ_2 is used to turn on the heat transfer equations gradually with values ranging from 0 to 1 to finish initializing each packed bed. The four-stage initialization/solution strategy takes approximately 65 CPU-seconds on an Intel Core i7-6500U processor to solve the discretized packed bed model.

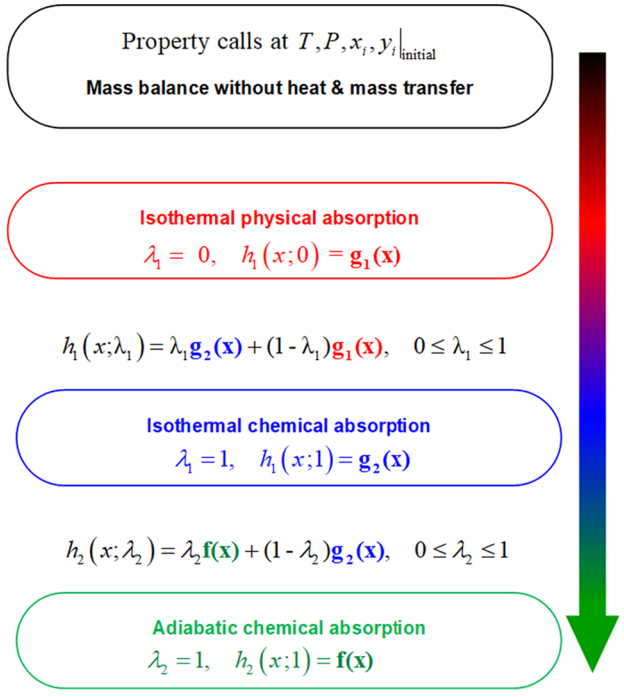

Figure 4. Packed bed initialization strategy.

The absorber column with three packed beds and two intercoolers is initialized as shown in Figure 5A. Each packed

https://doi.org/10.1021/acs.iecr.0c05035
Ind. Eng. Chem. Res. XXXX, XXX, XXX−XXX

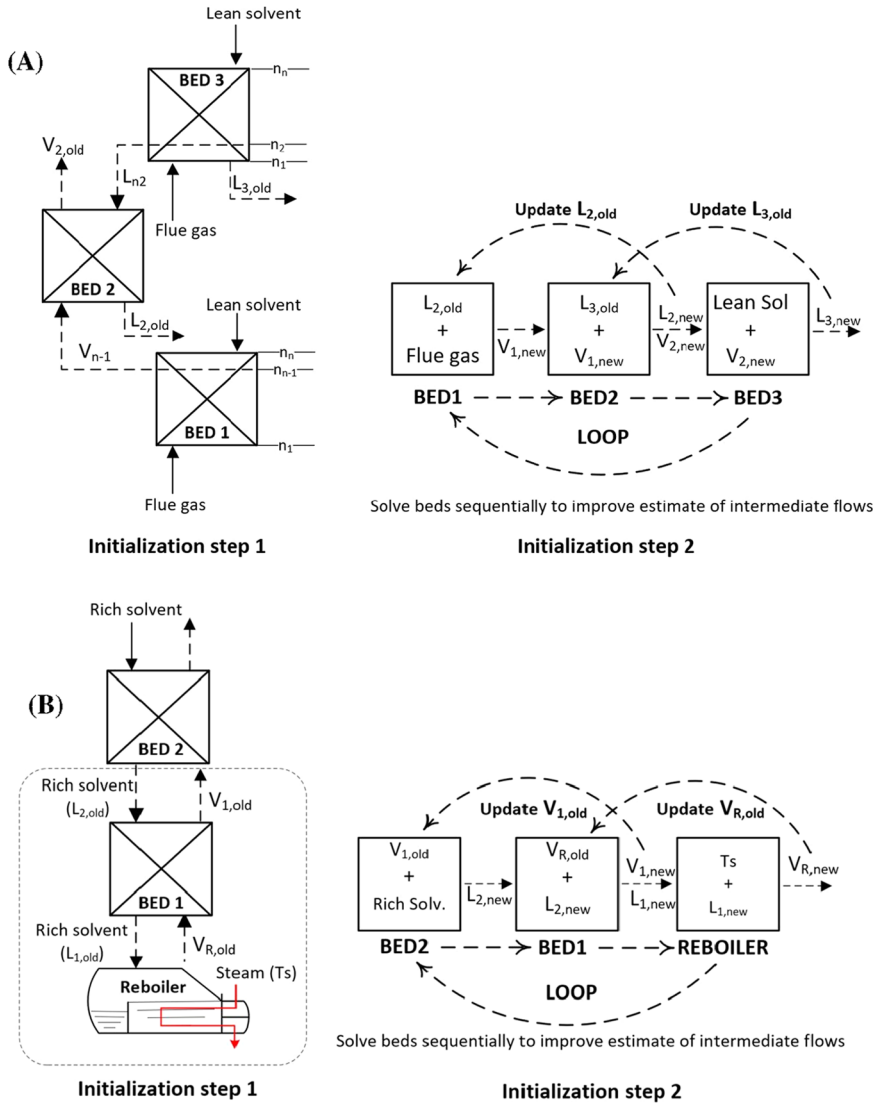

Figure 5. Initialization strategy: (A) absorber with three beds and (B) stripper with two beds and reboiler.

bed is solved sequentially using the strategy outlined to obtain good estimates of the flow, temperature, and composition of the intermediate flows. Finally, the three beds are solved together. Figure 5B shows the initialization procedure for the stripper and reboiler, where good initial estimates for the stream entering the reboiler are used to solve the reboiler model. The vapor generated is then used to solve the first and second packed beds of the stripper. The two packed beds and reboiler models are then solved sequentially to obtain good estimates before solving the three models together. The initialization procedure is found to enhance convergence of the plant-wide model when starting from initial estimates that are far from the solution. Once the solution of the plant-wide model is obtained, it is saved in a file for future use to avoid reinitialization.

4. RESULTS AND DISCUSSION

This section is subdivided into two main sections. Section 4.1 presents model validation with the experimental/industrial data. Section 4.2 presents optimization under off-design conditions.

4.1. Model Validation. Figure 6 shows the WWC model predictions and the measured CO_2 flux data from Dugas,[75] where the model simulation results are in the ±20% range. The overall agreement with the experimental data is deemed

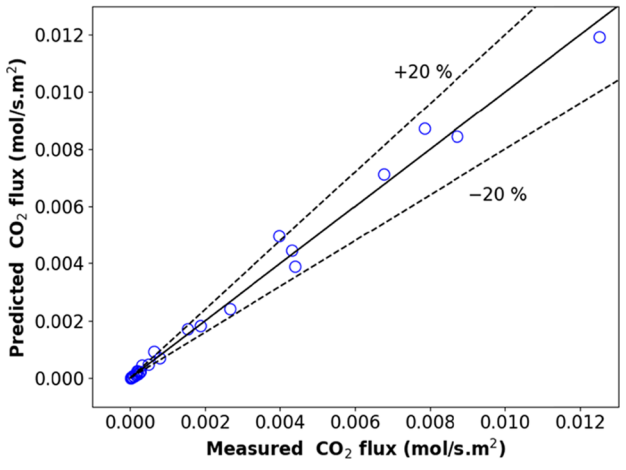

Figure 6. WWC parity plot.

https://doi.org/10.1021/acs.iecr.0c05035
Ind. Eng. Chem. Res. XXXX, XXX, XXX−XXX

adequate with a root-mean-square error of 6.4×10^{-5} mol/(m^2 s).

Considering data from NCCC, the prediction of CO_2 percentage in the absorber as shown in Table 5 compares

Table 5. Comparison of Absorber Model Predictions for CO_2 Capture Percentage with NCCC Data

case no	model prediction	gas-side NCCC data[a]	liquid-side NCCC data[b]	L/G (mol/mol)	LLD (mol CO_2/mol MEA)
1	99.98	99.91	89.45	3.75	0.14
2	99.88	99.49	93.26	6.25	0.25
3	73.89	78.57	70.86	1.75	0.08
4	99.99	99.53	90.69	3.72	0.11
5	67.60	59.03	58.89	3.54	0.35
6	99.97	98.07	93.92	6.67	0.15
7	53.50	55.48	52.30	1.68	0.24

[a]The gas-side CO_2 capture is defined as the ratio of the difference between CO_2 flowrates at the absorber inlet and outlet gas streams to the CO_2 flowrate at the absorber inlet gas stream. [b]The liquid-side CO_2 capture is defined as the ratio of the difference between the CO_2 flowrates at the absorber outlet and inlet liquid streams to the CO_2 flowrate at the absorber inlet gas stream (see eq S50 in the Supporting Information).

well with the experimental data, given that the largest deviation is 4% of CO_2 capture when compared with the data for the gas side. Details of these test runs can be found in the Supporting Information. It can be observed in Table 5 that cases 3 and 5 have the highest discrepancies. In an earlier paper[55] written by some of the authors of this paper, where these data were used for model validation by using an Aspen Plus-based model, it can be observed that for case 3 (case# K4 in that paper) and case 5 (case# K6 in that paper), model predictions were 76.5 and 68.16% CO_2 captures, respectively, using the deterministic model. The deterministic results for CO2 percentage capture from that study strongly agree with those obtained in this paper. Interestingly, when the uncertainty in composition measurement was taken into consideration in that paper,[55] model prediction for case 5 (case# K6 in that paper) became 60.59%, which is very close to the plant data. In the future, the authors look forward to incorporating and evaluating the effects of the measurement and model uncertainties on the predicted results.

Figure 7 shows the predicted liquid-phase temperature profiles of the absorber compared with NCCC pilot plant temperature measurements. The predicted temperature profile of case 3 (Figure 7A), where the L/G ratio is relatively low (1.75 mol/mol), agrees strongly with the measured data. In case 2, the L/G ratio is relatively high (6.25 mol/mol) resulting in the temperature bulge at the bottom of the column, as shown in Figure 7B, which suggests an increased absorption rate at this packing height.[129] Consequently, reactions in the liquid phase can deviate from the fast pseudo-first-order zone (where $E = Ha$) as the concentration of the free MEA at the interface differs from the bulk concentration. Hence, setting the enhancement factor to the Hatta number for absorption operation in this region can lead to errors as seen in Bed1 of B, where it is observed that the GM for the enhancement factor calculation differs significantly from the Hatta number. This behavior has also been reported by other authors.[34,67,73] Overall, the model prediction shows good agreement with the pilot plant data.

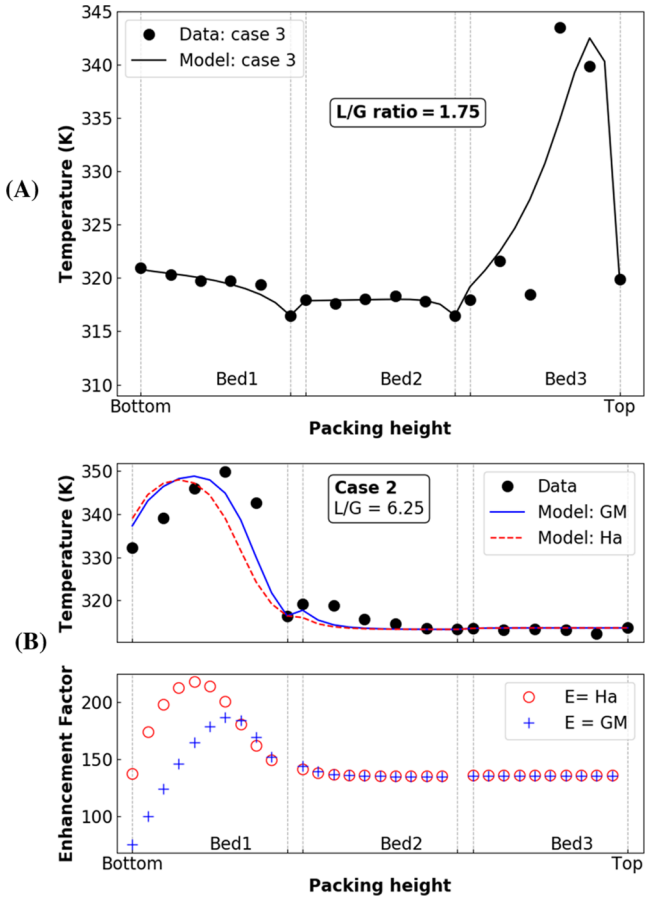

Figure 7. Comparison of absorber temperature profiles between the model and the NCCC data for (A) case 3 and (B) case 2 with Hatta number and GM model for the enhancement factor calculation.

Similarly, the temperature profile of the stripper is compared with the measured NCCC data for the desorption of CO_2, as shown in Figure 8A. Furthermore, the 2015 baseline data[80] of the TCM amine plant shown in Tables S20 and S21 are also used to validate the absorber and stripper columns, as shown in Figure 8B. The packing type used for the TCM packed bed is Koch Glitsch Flexipac 2X with a specific surface area of 225 m^2/m^3 and void fraction of 0.97. The temperature profile predicted by the model for both absorption and stripping operation for this specific test run is in good agreement with the plant data as shown in Figure 8B. For the corresponding CO_2 loading of the rich solvent leaving the absorber, the model has an absolute percentage deviation (APD) of 4.1%.

The RL-HX model predictions for the lean and rich solvent exit temperatures are consistent with the NCCC pilot plant data, as shown in Figure 9 (details of these test runs are in the Supporting Information). A hot-end approach temperature as low as 4 °C can be obtained as shown in Figure 9A using PHE. The PHE thermal model based on the ε-NTU approach converges reliably and is computationally efficient.

4.2. Part-Load Optimization Studies under Variable CO_2 Capture. To optimize the capture unit under steady-state part-load operations and variable capture, a reference plant is first designed. For all of the studies conducted in this section, the plant is assumed to be at steady state. The goal is

https://doi.org/10.1021/acs.iecr.0c05035
Ind. Eng. Chem. Res. XXXX, XXX, XXX−XXX

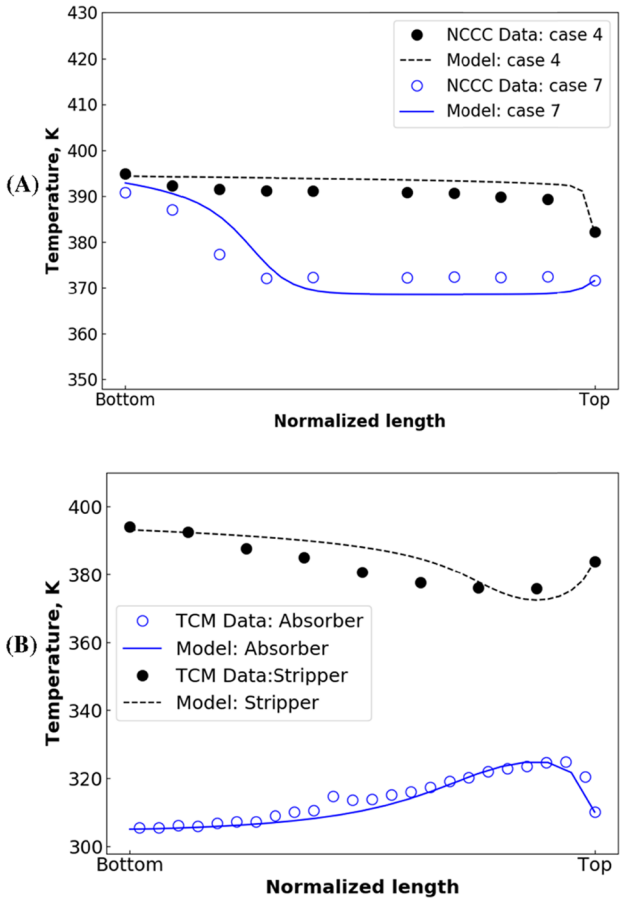

Figure 8. Comparison of model predictions with (A) NCCC stripper data and (B) TCM 2015 baseline data.

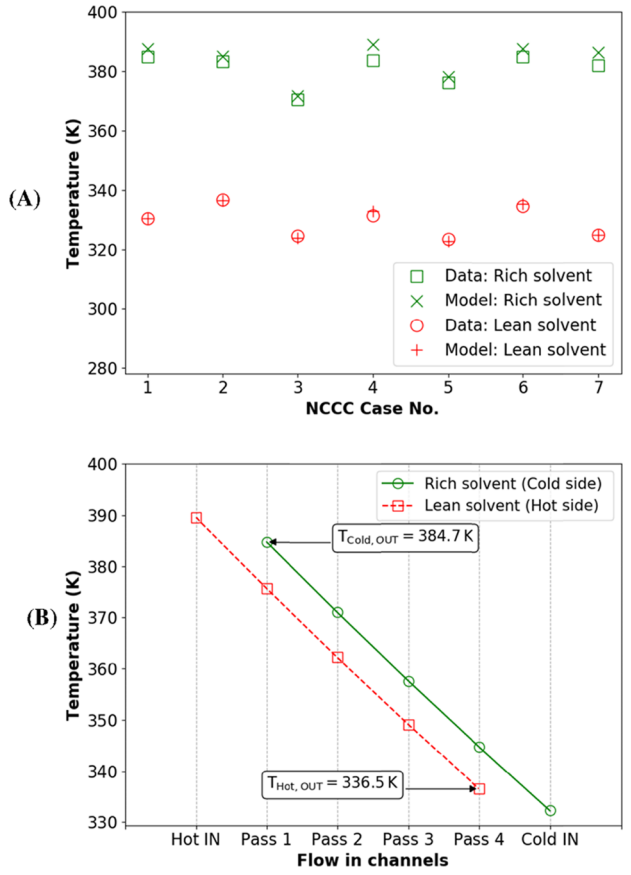

Figure 9. NCCC PHE predictions: (A) exit temperature and (B) channel temperature profile for case 2.

to determine the variation of the operating cost of the reference plant with CO_2 percentage capture and flue gas conditions. Two different flue gas compositions are considered: one is of higher CO_2 concentration similar to pulverized coal-fired power plants (PC) and another is of lower CO_2 concentration similar to natural gas-fired power plants (NGCC).

4.2.1. Configuration and Operating Range of Reference Amine Plant. For the reference plant, the flue gas compositions considered are similar to that at the CO_2 Technology Centre Mongstad (TCM) test facility. The TCM amine plant has the capacity of treating up to about 60 000 S m^3/h of flue gas from either a natural gas turbine-combined heat and power (CHP) plant or a residual fluidized catalytic cracker (RFCC) unit.[1] The CHP flue gas has a CO_2 composition of about 3−4 mol % comparable to NGCC, while the RFCC flue gas contains a higher CO_2 composition (13−14 mol %) similar to a PC power plant, as shown in Table 6[130,131] The packing height and diameter for the columns of the reference plant are set to the CHP configuration of the TCM amine plant. By retaining the four-pass-four-pass *Z*-configuration of the NCCC PHE, the total heat transfer area of the RL-HX for the reference plant is set to 308 m^2, similar to the PHE at the TCM plant.[27] This translates to a PHE with 28 channels per pass for each fluid. The design and operating parameters of the amine plant for the part-load and variable capture optimization studies are shown in Table 7.

Table 6. Typical Composition (mol %) of Flue Gas Stream at TCM

flue gas conditions	O_2	N_2 + Ar	CO_2	H_2O
high CO_2 composition ($y_{CO_2,HIGH}$)	3.2	77.9	14.7	4.2
low CO_2 composition ($y_{CO_2,LOW}$)	14.4	80.6	3.6	1.4

Table 7. Design and Operating Parameters of the Reference Plant

design specification	value
absorber diameter (m)	3
absorber packing height (m)	24
stripper diameter (m)	1.3
stripper packing height (m)	8
absorber/stripper packing type	MellapakPlus 252Y
PHE area of single plate (m^2)	1.38
PHE no. of passes	4
PHE channels per pass	28
operating parameters	**value**
MEA concentration (wt %)	30
lean solvent temperature (K)	308.15
absorber/stripper pressure (kPa)	101.3/175
condenser temperature (K)	303.15
flue gas temperature (K)	301.15
flue gas base load (100%) (kmol/s)	0.7049

Hence, given the aforementioned design and operating conditions of the reference plant, the optimization search space is defined by the range of operations for flue gas

https://doi.org/10.1021/acs.iecr.0c05035
Ind. Eng. Chem. Res. XXXX, XXX, XXX−XXX

flowrate, CO_2 capture percentage, lean solvent CO_2 loading, and CO_2 composition in flue gas, as given in Table 8

Table 8. Ranges of Key Process Parameters for Optimization Studies

process parameter	low	high
flue gas flowrate	60% base load	100% base load
CO_2 capture percentage	75%	90%
lean solvent CO_2 loading	0.1	0.4
CO_2 composition in flue gas (mol %)	3.7	14.7

The objective of the part-load optimization is to minimize the operating cost (OPC) defined in eq 17, which includes the cost of steam consumed in the reboiler, the cost of electricity required for pumping the lean and rich solvents, and the cost of cooling water required in the condenser and cooler. The pumping duty (Q_{pump}) is computed by assuming an overall efficiency of 75%. The reboiler duty is computed as described in Section 2.1. The cooling duty consists of the condenser and cooler duties. Costs of steam, electricity, and cooling water, given by c_s, c_e, and c_w, respectively, are shown in Table 9. These prices are obtained from Turton et al.[132]

Table 9. Utility Cost Data (Obtained from Turton et al.[132])

utility	cost
steam	$2.03/GJ
electricity	$0.0674/kWh
cooling water	$0.378/GJ

Costs of steam and cooling water are based on only the operating costs under the assumption that the capital investment required to build the generation facility has already been depreciated.[132] The selected steam price is based on the steam extracted from a low-pressure turbine (5 barg, 160 °C) with credit for electricity using a natural gas fuel source.[132] The price of cooling water is the utility cost for producing cooling water using a cooling tower with a supply and return temperature of 30 and 45 °C, respectively. Obviously, these prices will change depending on the cost of electricity used, location, design, technology, and other factors. The reader is referred to Turton et al.[132] for more details about the cost basis. The plant is assumed to operate for 8000 h per year ($t_{hr/yr}$)

$$\text{OPC (M\$/year)} = (c_s\dot{Q}_{reb} + c_w\dot{Q}_c + c_e\dot{Q}_{pump}) \times (t_{hr/yr}) \quad (17)$$

4.2.2. Effect of the RL-HX Temperature Approach on the Reboiler Duty. Rich solvent leaving the absorber needs to be efficiently heated for stripping CO_2, while lean solvent leaving the stripper needs to be cooled down to favor absorption. Thus, preheating the rich solvent in the RL-HX reduces the reboiler duty. Consequently, it also reduces the cooling duty for the lean solvent before it is sent to the absorber. As mentioned in Section 1.1, the hot-end temperature approach of the RL-HX is assumed to be fixed by several studies focused on operational optimization. The motivation behind the study presented in this subsection is to evaluate the impact of this assumption on the reboiler duty under an off-design operation scenario. First, we note that during off-design operations, the CO_2 loading in the rich and lean solvents as well as the solvent flowrate can vary significantly. However, the RL-HX has a fixed area. It may be possible to change the heat transfer area by adding or removing plates but that would require shutdown of the plant and therefore changing the area of RL-HX is not considered to be feasible during plant operations. Two largely different operating conditions are evaluated. Case I considers a case with low lean CO_2 loading, while case II considers a case with high lean CO_2 loading. Other conditions corresponding to these cases are shown in Figure 10A. For this study, only the

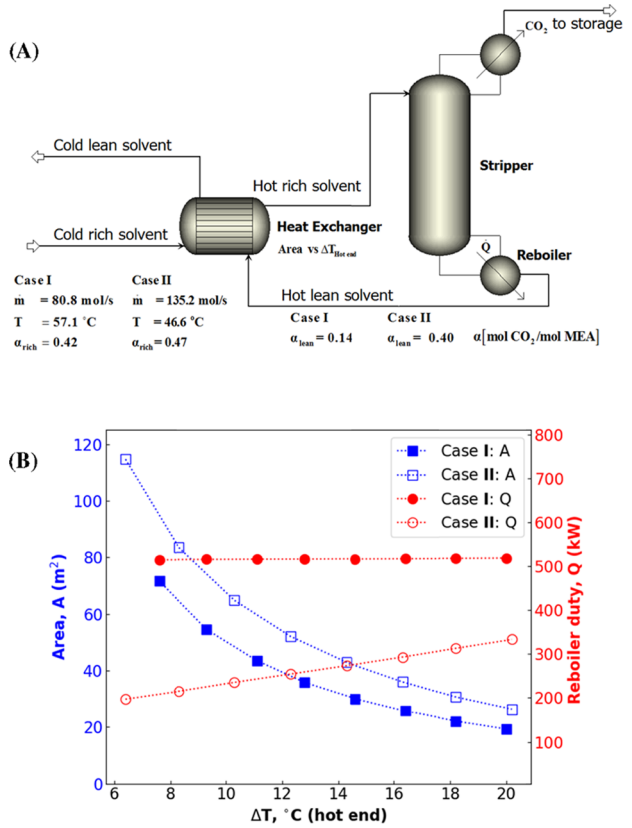

Figure 10. Fixed temperature approach analysis showing (A) PHE and stripper with operating conditions for two specific cases, (B) PHE area and reboiler duty with respect to the hot-end temperature approach for case I: low lean load scenario and case II: high lean loading scenario.

desorption section including the RL-HX is simulated, as shown in Figure 10A. The simulation is done using the models from the U.S. DOE's Carbon Capture Simulation Initiative (CCSI) toolset available for free download at https://github.com/CCSI-Toolset/MEA_ssm.

Figure 10B shows the variation of design area with the hot-end temperature approach and the variation of the reboiler duty with the hot-end temperature approach. It can be observed that at low lean solvent loading, a decrease in the hot-end temperature approach in the range studied here has only a minor effect on the reboiler duty. This is because at very low lean loading, the dominant contribution to the reboiler duty is the heat required for the endothermic reaction rather than the sensible heat. On the other hand, for high CO_2 lean loading, which leads to higher circulation rate such as in case II, the reboiler duty varies significantly with the hot-end temperature approach as the sensible heat

https://doi.org/10.1021/acs.iecr.0c05035
Ind. Eng. Chem. Res. XXXX, XXX, XXX−XXX

requirement for heating the large flow of circulating solvent constitutes a larger portion of the reboiler duty. In summary, the study shows that (i) the design area would differ depending on the design temperature approach and design operating conditions and (ii) the impact of the given design area (or the hot-end temperature approach) on the reboiler duty depends on the operating conditions. This study motivates consideration of a rigorous RL-HX model with a given heat transfer area rather than a fixed temperature approach for optimization under off-design operations.

4.2.3. Optimal Operating Conditions at Base Load. The L/G ratio is optimized by varying the lean solvent loading (LLD) to determine the circulation rate required to maintain the absorber performance at the given capture rate. Figure 11

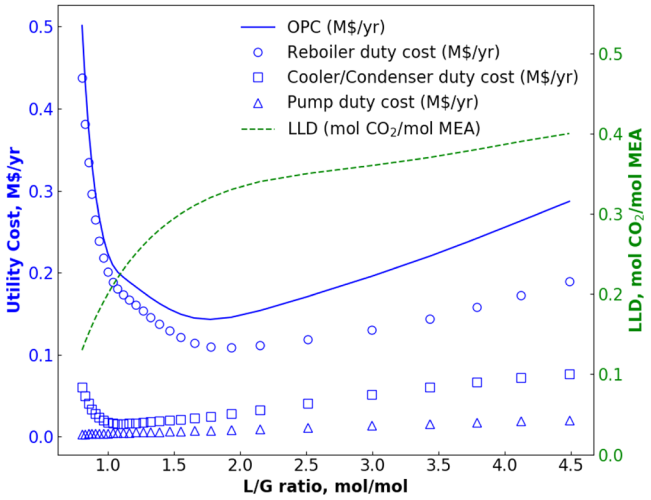

Figure 11. Utility cost at a 90% capture for varying the L/G (mol/mol) ratio at the base load of flue gas with low CO_2 inlet concentrations.

shows the sensitivity of OPC with respect to the L/G ratio at a 90% capture of low inlet CO_2 concentration flue gas at base load. The optimal L/G ratio is observed at about 1.78 mol/mol, and the OPC breakdown into reboiler duty, pumping duty, and cooling duty is also shown.

For a given capture rate, a lower L/G ratio requires a lower lean loading to satisfy the desired extent of CO_2 capture in the absorber. Figure 11 shows that as the L/G ratio becomes smaller than about 1.78 mol/mol, there is a steeper decrease in the desired lean loading. This leads to a steeper increase in the reboiler duty and a consequent steeper increase in the OPC, as shown in Figure 11. As the L/G ratio is increased beyond the optimal value, the reboiler duty keeps increasing, mainly due to the increasing requirement of sensible heat. The cooler/condenser duty follows a similar trend as the reboiler, i.e., increasing steeply when L/G is lower than optimal and a gradual increase when the L/G ratio is higher than the optimal value. Pumping cost monotonically keeps increasing with a higher L/G ratio as expected. Due to these cumulative effects, the OPC starts increasing when the L/G ratio is higher than optimal.

Figure 12 shows the utility costs at a 90% capture for varying L/G ratio required to treat flue gas with high CO_2 inlet concentrations at the base load. A higher optimum L/G ratio (~7.4 mol/mol) for treating flue gas with a 14.7 mol % CO_2 inlet concentration is obtained when compared with

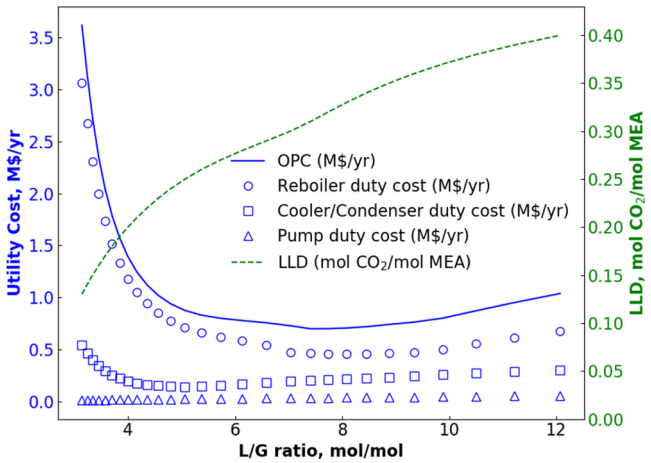

Figure 12. Utility cost at a 90% capture for varying L/G (mol/mol) ratio at the base load of flue gas with high CO_2 inlet concentrations.

that for flue gas with a 3.6 mol % composition. One key characteristic common to both Figures 11 and 12 is that the OPC increases steeply below the optimal L/G ratio showing the impact the L/G ratio has on the energy penalty. The study shows that operating the capture plant at the optimal L/G ratio will be highly desired for minimizing the operating cost.

4.2.4. Effect of Part-Load Operations on the RL-HX Temperature Approach. The RL-HX is developed as a PHE with the design parameters given in Table 8. Figure 13 shows

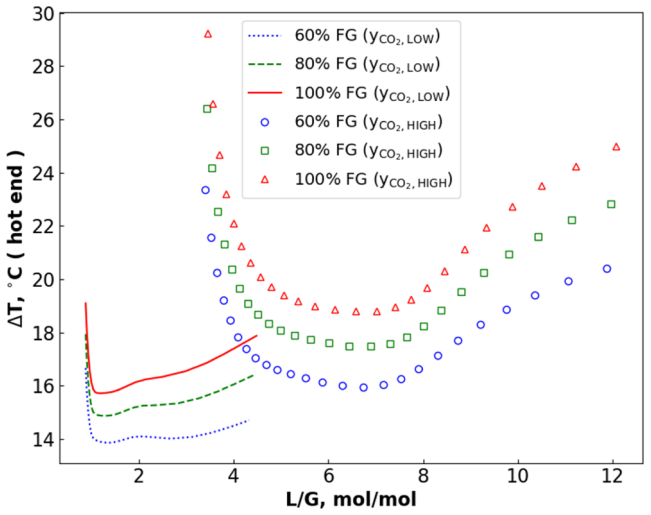

Figure 13. RL-HX temperature approach under part-load operations (60−100% base load) at a 90% CO_2 capture.

the hot-end temperature approach of the RL-HX under part-load operations and varying L/G ratio at a 90% capture for flue gas with high and low CO_2 compositions. It can be observed that the minimum $\Delta T_{\text{hot end}}$ at each part load for both the flue gas with low and high CO_2 contents is similar for the optimum L/G ratio. Also, a change in the flue gas load with a high CO_2 content from 100 to 60% results in a change in the minimum $\Delta T_{\text{hot end}}$ from 19 to 16 K, while that of the flue gas with low CO_2 content changed from 16 to 14 K. For other operating points, $\Delta T_{\text{hot end}}$ varies significantly depending on the lean loading, as explained in Section 4.2.2. The reduction in the energy penalty of the capture plant as a

https://doi.org/10.1021/acs.iecr.0c05035
Ind. Eng. Chem. Res. XXXX, XXX, XXX−XXX

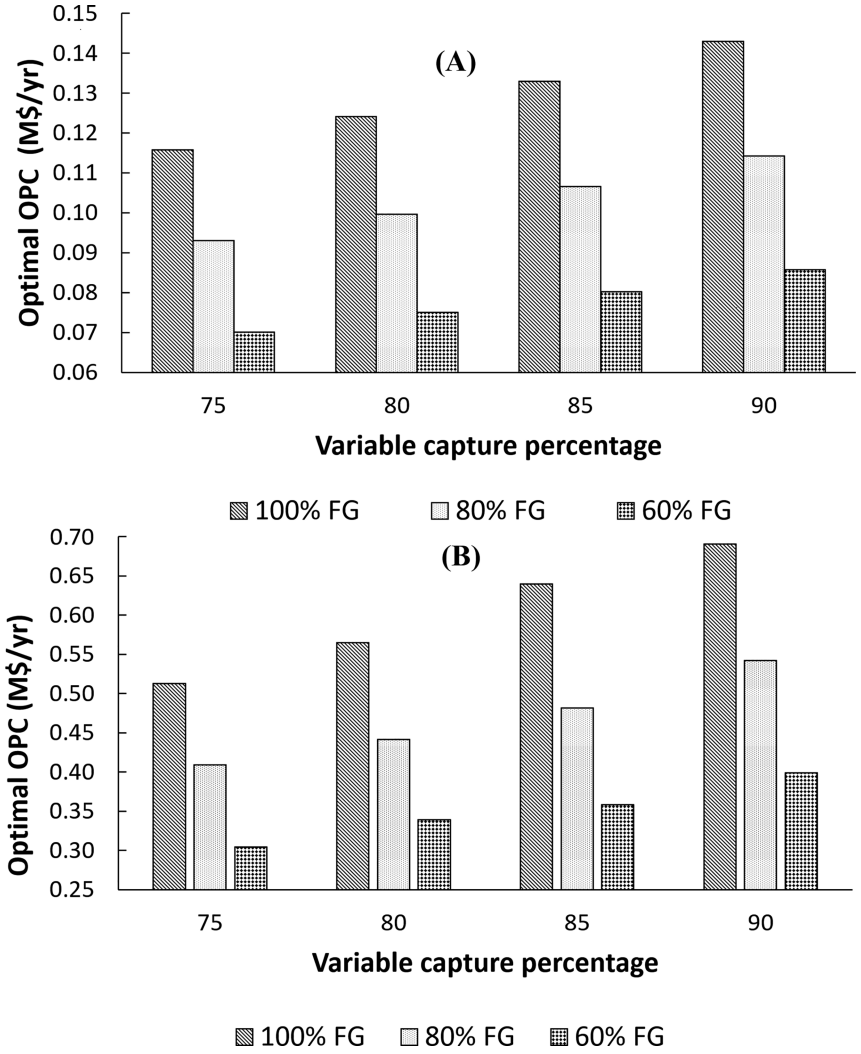

Figure 14. Optimal operating cost for variable flue gas load and percentage capture for (A) low CO_2 inlet composition and (B) high CO_2 inlet composition.

result of preheating the rich solvent in the RL-HX has a higher impact at higher lean loading when the solvent circulation rate is higher, thus requiring a higher amount of sensible heat.

4.2.5. Coupled Part-Load and Variable Capture Operations. The studies conducted here consider steady-state part-load and variable capture operations. Figure 14 shows a bar graph for the optimal OPC vs variable capture for flue gas with low and high CO_2 compositions at three distinct loads of 100, 80, and 60%. Once again, it should be noted that the optimal OPC reported in Figure 14 is based on eq 17 that only accounts for the total utility consumption. The optimal OPC reported in Figure 14 is for the corresponding capture rates. In reality, the desired capture rate would depend on many factors like carbon tax/credit, environmental policy, etc. Figure 14 shows that the optimal OPC for the flue gas with higher CO_2 concentrations (Figure 14B) is considerably higher compared to the corresponding cases for the flue gas with lower CO_2 concentrations (Figure 14A). This is because of higher utility consumption for the cases with higher CO_2 concentrations as the total amount of CO_2 captured is higher compared to the flue gas with low CO_2 concentrations. In addition, the optimal OPC keeps increasing with higher percentage capture for both low-concentration and high-concentration flue gases as the amount of CO_2 captured increases. Similarly, for a given percentage capture, the optimal OPC keeps increasing with higher loads.

Table 10 provides a summary of the optimal L/G ratios for each load and variable percentage capture. The flue gas with

Table 10. Optimal L/G (mol/mol) Ratios under Variable Flue Gas Loads (60, 80, and 100%) and CO_2 Removal Target (75 and 90%) at Two Different Flue Gas Concentrations[a]

	CO_2 percentage capture (%)	
flue gas load (%)	75	90
60 ($y_{CO_2, Low}$)	1.41	1.74
80 ($y_{CO_2, Low}$)	1.41	1.76
100 ($y_{CO_2, Low}$)	1.42	1.78
60 ($y_{CO_2, High}$)	5.94	7.16
80 ($y_{CO_2, High}$)	6.05	7.29
100 ($y_{CO_2, High}$)	6.49	7.40

[a] $y_{CO_2, Low}$ corresponds to 3.6 mol % CO_2 and $y_{CO_2, High}$ Is 14.7 mol %.

https://doi.org/10.1021/acs.iecr.0c05035
Ind. Eng. Chem. Res. XXXX, XXX, XXX−XXX

a higher CO_2 content corresponding to a pulverized coal power plant requires a higher L/G ratio compared to the NGCC flue gas with lower CO_2 content. For the same absorber column size and flue gas flowrate, the optimal required solvent flowrate at a given removal target reduces when treating flue gas with a lower CO_2 composition. It should be noted that this study has been conducted by considering the same equipment dimensions for treating both the high- and low-concentration flue gases and the plant hardware design is not necessarily optimal. The optimal OPC is likely to vary if the plant equipment items are optimally designed by considering the CO_2 concentration in the feed flue gas.

5. CONCLUSIONS

The IDAES computation platform is utilized to develop a detailed model of an amine-based CO_2 capture process. The initialization routine is found to lead to successful convergence of this highly nonlinear system starting with initial guesses that are far from the solution. Model results compare well with the data from the NCCC pilot plant, TCM pilot plant, and WWC experiments under considerable variation of solvent flowrate, gas flowrate, CO_2 concentration in the gas, variable capture rate, and steam flowrate to the reboiler as would be expected under off-design operations.

The plant-wide model is used for steady-state optimization of a reference capture unit under part-load operations and variable capture rates using flue gas similar to a pulverized coal and natural gas-combined cycle power plants. Analysis on the performance of the reference RL-HX showed that the hot-end temperature approach can considerably vary under off-design operations. Performance evaluation of the amine reference plant shows that the optimal operating conditions at base load are suboptimal for part-load and variable capture operations. The study shows that if L/G ratio keeps becoming lower than the optimal value, the energy penalty keeps becoming steeper. If the L/G ratio is higher than the optimal, the energy penalty also keeps increasing but the increase is much less steep than when the L/G ratio is lower than optimal. The optimal L/G ratio is found to be higher for capturing CO_2 from a flue gas with higher CO_2 concentration. For a given load, as the percentage capture is increased, the optimal L/G ratio is generally found to increase especially for the flue gas with a higher concentration of CO_2. The optimal OPC for the flue gas with higher CO_2 concentrations is found to be considerably higher compared to those for the flue gas with lower CO_2 concentrations for all loads and capture percentages that are evaluated. The optimal OPC increases as the percentage capture increases at a given load and as the load increases for a given percentage capture. These results for the optimal OPC are generated for a few specific capture percentages, but in an operating capture plant, there would be a CO_2 capture target that the plant needs to satisfy. It should also be noted that the OPC results presented are specific to the formulation considered in this work.

This study shows that the optimal operation of an existing capture unit is crucial to minimizing the parasitic energy loss in the capture plant under part-load and variable capture conditions. The studies conducted here consider the same equipment size for both low- and high-concentration flue gases. Furthermore, the equipment designs are not necessarily optimal. For improving the plant economics further, it will also be desired to optimally design the equipment items with due consideration of the part-load and variable capture operations as well as the CO_2 concentration in the incoming flue gas. Finally, the model described here is available for free download under https://github.com/IDAES/idaes-pse/tree/main/idaes/power_generation/carbon_capture/mea_solvent_system.

■ ASSOCIATED CONTENT

Supporting Information

The Supporting Information is available free of charge at https://pubs.acs.org/doi/10.1021/acs.iecr.0c05035.

Model equations for the packed column, reboiler, condenser, and plate heat exchanger; property model of the CO_2−MEA−H_2O system including the VLE model; correlations for mass transfer coefficients, interfacial area, vapor-phase heat transfer coefficient, and reaction rate constants; reconstitution of apparent species from true species; steady-state NCCC data; steady-state TCM data; and calculation of the percentage capture for the TCM data (PDF)

■ AUTHOR INFORMATION

Corresponding Author

Debangsu Bhattacharyya − *Department of Chemical and Biomedical Engineering, West Virginia University, Morgantown, West Virginia 26506, United States;* orcid.org/0000-0001-9957-7528; Phone: +1-3042939335; Email: Debangsu.Bhattacharyya@mail.wvu.edu; Fax: +1-3042934139

Authors

Paul Akula − *Department of Chemical and Biomedical Engineering, West Virginia University, Morgantown, West Virginia 26506, United States;* orcid.org/0000-0003-1050-976X

John Eslick − *National Energy Technology Laboratory, Pittsburgh, Pennsylvania 15236, United States*

David C. Miller − *National Energy Technology Laboratory, Pittsburgh, Pennsylvania 15236, United States;* orcid.org/0000-0002-7378-5625

Complete contact information is available at: https://pubs.acs.org/10.1021/acs.iecr.0c05035

Notes

This presentation was prepared as an account of work sponsored by an agency of the United States Government. Neither the United States Government nor any agency thereof, nor any of their employees, makes any warranty, express or implied, or assumes any legal liability or responsibility for the accuracy, completeness, or usefulness of any information, apparatus, product, or process disclosed, or represents that its use would not infringe privately owned rights. Reference herein to any specific commercial product, process, or service by trade name, trademark, manufacturer, or otherwise does not necessarily constitute or imply its endorsement, recommendation, or favoring by the United States Government or any agency thereof. The views and opinions of authors expressed herein do not necessarily state or reflect those of the United States Government or any agency thereof.

The authors declare no competing financial interest.

https://doi.org/10.1021/acs.iecr.0c05035
Ind. Eng. Chem. Res. XXXX, XXX, XXX−XXX

The corresponding documentation for the code can be found at https://idaes-pse.readthedocs.io/en/latest/technical_specs/model_libraries/power_generation/carbon_capture/mea_solvent_system/index.html

■ ACKNOWLEDGMENTS

This work was conducted as part of the Institute for the Design of Advanced Energy Systems (IDAES) with funding from the Simulation-Based Engineering Program of the U.S. Department of Energy's Office of Fossil Energy, Division of Cross-Cutting Research. Paul Akula thanks Joshua C. Morgan for technical support with the CCSI toolset for the Aspen Plus MEA model and the Petroleum Technology Development Fund (PTDF) for their scholarship support.

■ NOMENCLATURE

a_e	effective interfacial area per unit packed volume, m^2/m^3
a_p	interfacial area of packing, m^2/m^3
A	area, m^2
C	concentration, mol/m^3
$\hat{C}_p$	mean specific heat capacity, J/mol • K
c_s,c_e,c_w	cost of utilities, s = steam, e = electricity, w = cooling water
CHP	combined heat and power
D	Fick diffusion coefficient, m^2/s
d	diameter, m
E	enhancement factor
E^*_∞	instantaneous enhancement factor
F	molar flowrate, mol/s
G	mass flow velocity, $kg/(m^2\ s)$
h	heat transfer coefficient, $W/(m^2\ K)$
h'	heat transfer coefficient corrected for high mass flux, $W/(m^2\ K)$
He	Henry's constant, Pa m^3/mol
Ha	Hatta number
k	mass transfer coefficient, m/s
k'	mass transfer coefficient, $mol/(m^2\ s\ Pa)$
K	concentration-based equilibrium constant, m^3/mol
k_{rx}	overall reaction rate constant, $m^3/(mol\ s)$
L	length, m
OPC	operating cost, M$/year
P	pressure, Pa
$\dot{Q}$	heat duty, W
r	MEA−H_2O ratio
RFCC	residual fluidized catalytic cracker
SRD	specific reboiler duty, MJ/kg CO_2
T	temperature, K
u	superficial velocity, m/s
x	liquid-phase composition
y	vapor-phase composition
z	axial coordinate, m

■ GREEK SYMBOLS

ρ	molar density, mol/m^3
$\bar{\rho}$	density, kg/m^3
γ	activity coefficient
Υ	dimensionless concentration in enhancement factor model
λ	thermal conductivity, W/(m K)
λ_s	latent heat of steam, J/kg
λ_1,λ_2	homotopy parameters
α	lean solvent loading, mol CO_2/mol MEA

■ SUBSCRIPTS AND SUPERSCRIPTS

*	interface
a	apparent specie
b	bulk phase
t	true specie
V	vapor phase
L	liquid phase
i	component index
tot	total
z	axial domain
reb	reboiler
cond	condenser

■ REFERENCES

(1) Hamborg, E. S.; Smith, V.; Cents, T.; Brigman, N.; Falk-Pedersen, O.; De Cazenove, T.; Chhaganlal, M.; Feste, J. K.; Ullestad, Ø.; Ulvatn, H.; et al. Results from MEA testing at the CO2 Technology Centre Mongstad. Part II: Verification of baseline results. *Energy Procedia* **2014**, *63*, 5994−6011.

(2) Bui, M.; Adjiman, C. S.; Bardow, A.; Anthony, E. J.; Boston, A.; Brown, S.; Fennell, P. S.; Fuss, S.; Galindo, A.; Hackett, L. A.; et al. Carbon capture and storage (CCS): the way forward. *Energy Environ. Sci.* **2018**, *11*, 1062−1176.

(3) Stec, M.; Tatarczuk, A.; Więcław-Solny, L.; Krótki, A.; Spietz, T.; Wilk, A.; Śpiewak, D. Demonstration of a post-combustion carbon capture pilot plant using amine-based solvents at the Łaziska Power Plant in Poland. *Clean Technol. Environ. Policy* **2016**, *18*, 151−160.

(4) Edenhofer, O. *Climate Change 2014: Mitigation of Climate Change*; Cambridge University Press, 2015; Vol. 3.

(5) Wang, M.; Lawal, A.; Stephenson, P.; Sidders, J.; Ramshaw, C. Post-combustion CO2 capture with chemical absorption: A state-of-the-art review. *Chem. Eng. Res. Des.* **2011**, *89*, 1609−1624.

(6) Supekar, S. D.; Skerlos, S. J. Reassessing the efficiency penalty from carbon capture in coal-fired power plants. *Environ. Sci. Technol.* **2015**, *49*, 12576−12584.

(7) Smith, N.; Miller, G.; Aandi, I.; Gadsden, R.; Davison, J. Performance and costs of CO2 capture at gas fired power plants. *Energy Procedia* **2013**, *37*, 2443−2452.

(8) Roeder, V.; Kather, A. Part Load Behaviour of Power Plants with a Retrofitted Post-combustion CO2 Capture Process. *Energy Procedia* **2014**, *51*, 207−216.

(9) Sarda, P.; Hedrick, E.; Reynolds, K.; Bhattacharyya, D.; Zitney, S. E.; Omell, B. Development of a dynamic model and control system for load-following studies of supercritical pulverized coal power plants. *Processes* **2018**, *6*, No. 226.

(10) Bankole, T.; Jones, D.; Bhattacharyya, D.; Turton, R.; Zitney, S. E. Optimal scheduling and its Lyapunov stability for advanced load-following energy plants with CO2 capture. *Comput. Chem. Eng.* **2018**, *109*, 30−47.

(11) Heuberger, C. F.; Mac Dowell, N. Real-World Challenges with a Rapid Transition to 100% Renewable Power Systems. *Joule* **2018**, *2*, 367−370.

(12) Hanak, D. P.; Biliyok, C.; Manovic, V. Evaluation and Modeling of Part-Load Performance of Coal-Fired Power Plant with Postcombustion CO_2 Capture. *Energy Fuels* **2015**, *29*, 3833−3844.

(13) Bui, M.; Gunawan, I.; Verheyen, V.; Feron, P.; Meuleman, E.; Adeloju, S. Dynamic modelling and optimisation of flexible operation in post-combustion CO_2 capture plants—A review. *Comput. Chem. Eng.* **2014**, *61*, 245−265.

(14) He, Z.; Sahraei, M. H.; Ricardez-Sandoval, L. A. Flexible operation and simultaneous scheduling and control of a CO_2 capture plant using model predictive control. *Int. J. Greenhouse Gas Control* **2016**, *48*, 300−311.

https://doi.org/10.1021/acs.iecr.0c05035
Ind. Eng. Chem. Res. XXXX, XXX, XXX−XXX

(15) Mac Dowell, N.; Shah, N. The multi-period optimisation of an amine-based CO_2 capture process integrated with a super-critical coal-fired power station for flexible operation. *Comput. Chem. Eng.* **2015**, *74*, 169−183.
(16) Chikukwa, A.; Enaasen, N.; Kvamsdal, H. M.; Hillestad, M. Dynamic modeling of post-combustion CO_2 capture using amines−a review. *Energy Procedia* **2012**, *23*, 82−91.
(17) Llano-Restrepo, M.; Araujo-Lopez, E. Modeling and simulation of packed-bed absorbers for post-combustion capture of carbon dioxide by reactive absorption in aqueous monoethanolamine solutions. *Int. J. Greenhouse Gas Control* **2015**, *42*, 258−287.
(18) Krishnamurthy, R.; Taylor, R. A nonequilibrium stage model of multicomponent separation processes. Part I: model description and method of solution. *AIChE J.* **1985**, *31*, 449−456.
(19) Taylor, R.; Kooijman, H. A.; Hung, J. S. A second generation nonequilibrium model for computer simulation of multicomponent separation processes. *Comput. Chem. Eng.* **1994**, *18*, 205−217.
(20) Klöker, M.; Kenig, E. Y.; Hoffmann, A.; Kreis, P.; Górak, A. Rate-based modelling and simulation of reactive separations in gas/vapour−liquid systems. *Chem. Eng. Process.* **2005**, *44*, 617−629.
(21) Kenig, E. Y.; Górak, A.; Pyhälahti, A.; Jakobsson, K.; Aittamaa, J.; Sundmacher, K. Advanced rate-based simulation tool for reactive distillation. *AIChE J.* **2004**, *50*, 322−342.
(22) Kenig, E.; Górak, A. A film model based approach for simulation of multicomponent reactive separation. *Chem. Eng. Process.* **1995**, *34*, 97−103.
(23) Kenig, E. Y.; Wiesner, U.; Górak, A. Modeling of Reactive Absorption Using the Maxwell−Stefan Equations. *Ind. Eng. Chem. Res.* **1997**, *36*, 4325−4334.
(24) Pandya, J. Adiabatic gas absorption and stripping with chemical reaction in packed towers. *Chem. Eng. Commun.* **1983**, *19*, 343−361.
(25) Patron, G. D.; Ricardez-Sandoval, L. A robust nonlinear model predictive controller for a post-combustion CO_2 capture absorber unit. *Fuel* **2020**, *265*, No. 116932.
(26) Zaman, M.; Lee, J. H. Optimization of the various modes of flexible operation for post-combustion CO_2 capture plant. *Comput. Chem. Eng.* **2015**, *75*, 14−27.
(27) Montañés, R. M.; Fløa, N. E.; Nord, L. O. Dynamic process model validation and control of the amine plant at CO_2 Technology Centre Mongstad. *Energies* **2017**, *10*, No. 1527.
(28) Gáspár, J.; Cormoş, A.-M. Dynamic modeling and validation of absorber and desorber columns for post-combustion CO_2 capture. *Comput. Chem. Eng.* **2011**, *35*, 2044−2052.
(29) Harun, N.; Nittaya, T.; Douglas, P. L.; Croiset, E.; Ricardez-Sandoval, L. A. Dynamic simulation of MEA absorption process for CO_2 capture from power plants. *Int. J. Greenhouse Gas Control* **2012**, *10*, 295−309.
(30) Gabrielsen, J.; Michelsen, M. L.; Stenby, E. H.; Kontogeorgis, G. M. Modeling of CO2 absorber using an AMP solution. *AIChE J.* **2006**, *52*, 3443−3451.
(31) Fløa, N. E.; Knuutila, H.; Kvamsdal, H. M.; Hillestad, M. Dynamic model validation of the post-combustion CO 2 absorption process. *Int. J. Greenhouse Gas Control* **2015**, *41*, 127−141.
(32) Tobiesen, F. A.; Juliussen, O.; Svendsen, H. F. Experimental validation of a rigorous desorber model for post-combustion capture. *Chem. Eng. Sci.* **2008**, *63*, 2641−2656.
(33) Kvamsdal, H. M.; Jakobsen, J. P.; Hoff, K. A. Dynamic modeling and simulation of a CO2 absorber column for post-combustion CO_2 capture. *Chem. Eng. Process.* **2009**, *48*, 135−144.
(34) Gaspar, J.; Fosbøl, P. L. A general enhancement factor model for absorption and desorption systems: A CO2 capture case-study. *Chem. Eng. Sci.* **2015**, *138*, 203−215.
(35) Dang, H.; Rochelle, G. T. CO_2 absorption rate and solubility in monoethanolamine/piperazine/water. *Sep. Sci. Technol.* **2003**, *38*, 337−357.
(36) van Krevelen, D.; Hoftijzer, P. Kinetics of gas-liquid reactions part I. General theory. *Recl. Trav. Chim. Pays-Bas* **1948**, *67*, 563−586.
(37) Savage, D. W.; Astarita, G.; Joshi, S. Chemical absorption and desorption of carbon dioxide from hot carbonate solutions. *Chem. Eng. Sci.* **1980**, *35*, 1513−1522.
(38) Wellek, R.; Brunson, R.; Law, F. Enhancement factors for gas-absorption with second-order irreversible chemical reaction. *Can. J. Chem. Eng.* **1978**, *56*, 181−186.
(39) Edwards, W. In *Section 14 in Perry s Chemical Engineering Handbook*; Perry, R. H.; Green, D. W.; Maloney, J. O., Eds.; McGraw-Hill Book Co.: New York, NY, 1984.
(40) DeCoursey, W. Absorption with chemical reaction: development of a new relation for the Danckwerts model. *Chem. Eng. Sci.* **1974**, *29*, 1867−1872.
(41) Porter, K. Effect of contact-time distribution on gas absorption with chemical reaction. *Trans. Inst. Chem. Eng. Chem. Eng.* **1966**, *44*, T25.
(42) Miller, D. C.; Siirola, J. D.; Agarwal, D.; Burgard, A. P.; Lee, A.; Eslick, J. C.; Nicholson, B.; Laird, C.; Biegler, L. T.; Bhattacharyya, D. et al. Next Generation Multi-Scale Process Systems Engineering Framework. *Computer Aided Chemical Engineering*; Elsevier: 2018; Vol. *44*, pp 2209−2214.
(43) Hart, W. E.; Laird, C. D.; Watson, J.-P.; Woodruff, D. L.; Hackebeil, G. A.; Nicholson, B. L.; Siirola, J. D. *Pyomo—Optimization Modeling in Python*; Springer, 2017; Vol. *67*.
(44) Biegler, L. T.; Zavala, V. M. Large-scale nonlinear programming using IPOPT: An integrating framework for enterprise-wide dynamic optimization. *Comput. Chem. Eng.* **2009**, *33*, 575−582.
(45) Akula, P.; Eslick, J.; Bhattacharyya, D.; Miller, D. C. Modelling and Parameter Estimation of a Plate Heat Exchanger as Part of a Solvent-Based Post-Combustion CO_2 Capture System. In *Computer Aided Chemical Engineering*; Muñoz, S. G.; Laird, C. D.; Realff, M. J., Eds.; Elsevier, 2019; Vol. *47*, pp 47−52.
(46) Lin, Y.-J.; Rochelle, G. T. Heat Transfer Enhancement and Optimization of Lean/Rich Solvent Cross Exchanger for Amine Scrubbing. *Energy Procedia* **2017**, *114*, 1890−1903.
(47) Freguia, S.; Rochelle, G. T. Modeling of CO2 capture by aqueous monoethanolamine. *AIChE J.* **2003**, *49*, 1676−1686.
(48) Li, K.; Leigh, W.; Feron, P.; Yu, H.; Tade, M. Systematic study of aqueous monoethanolamine (MEA)-based CO2 capture process: techno-economic assessment of the MEA process and its improvements. *Appl. Energy* **2016**, *165*, 648−659.
(49) Ziaii, S.; Rochelle, G. T.; Edgar, T. F. Dynamic Modeling to Minimize Energy Use for CO2 Capture in Power Plants by Aqueous Monoethanolamine. *Ind. Eng. Chem. Res.* **2009**, *48*, 6105−6111.
(50) Oyenekan, B. A.; Rochelle, G. T. Energy Performance of Stripper Configurations for CO2 Capture by Aqueous Amines. *Ind. Eng. Chem. Res.* **2006**, *45*, 2457−2464.
(51) Nittaya, T.; Douglas, P. L.; Croiset, E.; Ricardez-Sandoval, L. A. Dynamic modeling and evaluation of an industrial-scale CO2 capture plant using monoethanolamine absorption processes. *Ind. Eng. Chem. Res.* **2014**, *53*, 11411−11426.
(52) Jayarathna, S. A.; Lie, B.; Melaaen, M. C. Amine based CO2 capture plant: Dynamic modeling and simulations. *Int. J. Greenhouse Gas Control* **2013**, *14*, 282−290.
(53) Gunnarsson, J.; Sinclair, I.; Alanis, F. J. Compact heat exchangers: improving heat recovery: these units offer distinct advantages over shell-and-tube heat exchangers, as quantified by the example presented here. *Chem. Eng.* **2009**, *116*, 44−48.
(54) Chapel, D. G.; Mariz, C. L.; Ernest, J. In *Recovery of CO_2 from Flue Gases: Commercial Trends*, Canadian Society of Chemical Engineers Annual Meeting, Saskatchewan, Canada, 1999.
(55) Morgan, J. C.; Soares Chinen, A.; Omell, B.; Bhattacharyya, D.; Tong, C.; Miller, D. C.; Buschle, B.; Lucquiaud, M. Development of a Rigorous Modeling Framework for Solvent-Based CO2 Capture. Part 2: Steady-State Validation and Uncertainty Quantification with Pilot Plant Data. *Ind. Eng. Chem. Res.* **2018**, *57*, 10464−10481.
(56) Arce, A.; Mac Dowell, N.; Shah, N.; Vega, L. F. Flexible operation of solvent regeneration systems for CO_2 capture processes

https://doi.org/10.1021/acs.iecr.0c05035
Ind. Eng. Chem. Res. XXXX, XXX, XXX−XXX

using advanced control techniques: Towards operational cost minimisation. *Int. J. Greenhouse Gas Control* **2012**, *11*, 236−250.
(57) Galindo, A.; Whitehead, P. J.; Jackson, G.; Burgess, A. N. The thermodynamics of mixtures and the corresponding mixing rules in the SAFT-VR approach for potentials of variable range. *Mol. Phys.* **1998**, *93*, 241−252.
(58) Soares Chinen, A.; Morgan, J. C.; Omell, B.; Bhattacharyya, D.; Tong, C.; Miller, D. C. Development of a Rigorous Modeling Framework for Solvent-Based CO2 Capture. 1. Hydraulic and Mass Transfer Models and Their Uncertainty Quantification. *Ind. Eng. Chem. Res.* **2018**, *57*, 10448−10463.
(59) De Brito, M. H.; Von Stockar, U.; Bangerter, A. M.; Bomio, P.; Laso, M. Effective mass-transfer area in a pilot plant column equipped with structured packings and with ceramic rings. *Ind. Eng. Chem. Res.* **1994**, *33*, 647−656.
(60) Eslick, J. C.; Akula, P.; Bhattacharyya, D.; Miller, D. C. Simultaneous Parameter Estimation in Reactive-Solvent-Based Processes. *Computer Aided Chemical Engineering*; Elsevier, 2018; pp 901−906.
(61) Morgan, J. C.; Chinen, A. S.; Anderson-Cook, C.; Tong, C.; Carroll, J.; Saha, C.; Omell, B.; Bhattacharyya, D.; Matuszewski, M.; Bhat, K. S.; Miller, D. C. Development of a framework for sequential Bayesian design of experiments: Application to a pilot-scale solvent-based CO2 capture process. *Applied Energy* **2020**, *262*, No. 114533.
(62) Dugas, R. E. Pilot Plant Study of Carbon Dioxide Capture by Aqueous Monoethanolamine. MSE Thesis, University of Texas at Austin, 2006.
(63) Zhang, Y.; Chen, H.; Chen, C.-C.; Plaza, J. M.; Dugas, R.; Rochelle, G. T. Rate-based process modeling study of CO2 capture with aqueous monoethanolamine solution. *Ind. Eng. Chem. Res.* **2009**, *48*, 9233−9246.
(64) Lawal, A.; Wang, M.; Stephenson, P.; Koumpouras, G.; Yeung, H. Dynamic modelling and analysis of post-combustion CO2 chemical absorption process for coal-fired power plants. *Fuel* **2010**, *89*, 2791−2801.
(65) Biliyok, C.; Lawal, A.; Wang, M.; Seibert, F. Dynamic modelling, validation and analysis of post-combustion chemical absorption CO2 capture plant. *Int. J. Greenhouse Gas Control* **2012**, *9*, 428−445.
(66) Sønderby, T. L.; Carlsen, K. B.; Fosbøl, P. L.; Kiørboe, L. G.; von Solms, N. A new pilot absorber for CO2 capture from flue gases: Measuring and modelling capture with MEA solution. *Int. J. Greenhouse Gas Control* **2013**, *12*, 181−192.
(67) Tobiesen, F. A.; Svendsen, H. F.; Juliussen, O. Experimental validation of a rigorous absorber model for CO2 postcombustion capture. *AIChE J.* **2007**, *53*, 846−865.
(68) Bui, M.; Tait, P.; Lucquiaud, M.; Mac Dowell, N. Dynamic operation and modelling of amine-based CO2 capture at pilot scale. *Int. J. Greenhouse Gas Control* **2018**, *79*, 134−153.
(69) Bui, M.; Flø, N. E.; de Cazenove, T.; Mac Dowell, N. Demonstrating flexible operation of the Technology Centre Mongstad (TCM) CO_2 capture plant. *Int. J. Greenhouse Gas Control* **2020**, *93*, No. 102879.
(70) Cousins, A.; Wardhaugh, L.; Cottrell, A. Pilot Plant Operation for Liquid Absorption-Based Post-Combustion CO_2 Capture. In *Absorption-Based Post-Combustion Capture of Carbon Dioxide*; Feron, P. H. M., Ed.; Woodhead Publishing, 2016; Chapter 26, pp 649−684.
(71) Puxty, G.; Rowland, R.; Attalla, M. Comparison of the rate of CO2 absorption into aqueous ammonia and monoethanolamine. *Chem. Eng. Sci.* **2010**, *65*, 915−922.
(72) Karlsson, H.; Svensson, H. Rate of absorption for CO2 absorption systems using a wetted wall column. *Energy Procedia* **2017**, *114*, 2009−2023.
(73) Luo, X.; Hartono, A.; Hussain, S.; Svendsen, H. F. Mass transfer and kinetics of carbon dioxide absorption into loaded aqueous monoethanolamine solutions. *Chem. Eng. Sci.* **2015**, *123*, 57−69.
(74) Servia, A.; Laloue, N.; Grandjean, J.; Rode, S.; Roizard, C. Modeling of the CO2 absorption in a wetted Wall column by piperazine solutions. *Oil Gas Sci. Technol.-Rev. Inst. Fr. Pet.* **2014**, *69*, 885−902.
(75) Dugas, R. E. Carbon Dioxide Absorption, Desorption, and Diffusion in Aqueous Piperazine and Monoethanolamine. Doctoral Dissertation, University of Texas at Austin, 2009.
(76) Chinen, A. S.; Morgan, J. C.; Omell, B. P.; Bhattacharyya, D.; Miller, D. C. Dynamic data reconciliation and model validation of a MEA-based CO2 capture system using pilot plant data. *IFAC-PapersOnLine* **2016**, *49*, 639−644.
(77) Zhang, R.; Bonnin-Nartker, E. P.; Farthing, G. A.; Ji, L.; Klidas, M. G.; Nelson, M. E.; Rimpf, L. M. RSAT process development for post-combustion CO2 capture: Scale-up from laboratory and pilot test data to commercial process design. *Energy Procedia* **2011**, *4*, 1660−1667.
(78) Simon, L. L.; Elias, Y.; Puxty, G.; Artanto, Y.; Hungerbuhler, K. Rate based modeling and validation of a carbon-dioxide pilot plant absorbtion column operating on monoethanolamine. *Chem. Eng. Res. Des.* **2011**, *89*, 1684−1692.
(79) Plaza, J. M.; Rochelle, G. T. Modeling pilot plant results for CO2 capture by aqueous piperazine. *Energy Procedia* **2011**, *4*, 1593−1600.
(80) Faramarzi, L.; Thimsen, D.; Hume, S.; Maxon, A.; Watson, G.; Pedersen, S.; Gjernes, E.; Fostås, B. F.; Lombardo, G.; Cents, T.; et al. Results from MEA testing at the CO_2 Technology Centre Mongstad: Verification of baseline results in 2015. *Energy Procedia* **2017**, *114*, 1128−1145.
(81) Bhattacharyya, D.; Miller, D. Post-combustion CO_2 capture technologies — a review of processes for solvent-based and sorbent-based CO_2 capture. *Curr. Opin. Chem. Eng.* **2017**, *17*, 78−92.
(82) Cohen, S. M.; Rochelle, G. T.; Webber, M. E. Optimizing post-combustion CO2 capture in response to volatile electricity prices. *Int. J. Greenhouse Gas Control* **2012**, *8*, 180−195.
(83) Cohen, S. M.; Rochelle, G. T.; Webber, M. E. Turning CO_2 capture on and off in response to electric grid demand: A baseline analysis of emissions and economics. *J. Energy Resour. Technol.* **2010**, *132*, No. 021003.
(84) Mechleri, E.; Fennell, P. S.; Dowell, N. M. Optimisation and evaluation of flexible operation strategies for coal- and gas-CCS power stations with a multi-period design approach. *Int. J. Greenhouse Gas Control* **2017**, *59*, 24−39.
(85) Chalmers, H.; Gibbins, J.; Leach, M. Valuing power plant flexibility with CCS: the case of post-combustion capture retrofits. *Mitigation Adapt. Strategies Global Change* **2012**, *17*, 621−649.
(86) Chalmers, H.; Lucquiaud, M.; Gibbins, J.; Leach, M. Flexible operation of coal fired power plants with postcombustion capture of carbon dioxide. *J. Environ. Eng.* **2009**, *135*, 449−458.
(87) Rao, A. B.; Rubin, E. S. Identifying cost-effective CO2 control levels for amine-based CO2 capture systems. *Ind. Eng. Chem. Res.* **2006**, *45*, 2421−2429.
(88) Haines, M.; Davison, J. Designing carbon capture power plants to assist in meeting peak power demand. *Energy Procedia* **2009**, *1*, 1457−1464.
(89) Cohen, S. M.; Rochelle, G. T.; Webber, M. E. Optimal operation of flexible post-combustion CO2 capture in response to volatile electricity prices. *Energy Procedia* **2011**, *4*, 2604−2611.
(90) Ziaii, S.; Cohen, S.; Rochelle, G. T.; Edgar, T. F.; Webber, M. E. Dynamic operation of amine scrubbing in response to electricity demand and pricing. *Energy Procedia* **2009**, *1*, 4047−4053.
(91) Gibbins, J.; Crane, R.; Lambropoulos, D.; Booth, C.; Roberts, C.; Lord, M. Maximising the Effectiveness of Post Combustion CO_2 Capture Systems. *Greenhouse Gas Control Technologies*; Elsevier, 2005; Vol. 7, pp 139−146.
(92) Mac Dowell, N.; Shah, N. Optimisation of post-combustion CO2 capture for flexible operation. *Energy Procedia* **2014**, *63*, 1525−1535.

https://doi.org/10.1021/acs.iecr.0c05035
Ind. Eng. Chem. Res. XXXX, XXX, XXX−XXX

(93) Alie, C.; Backham, L.; Croiset, E.; Douglas, P. L. Simulation of CO2 capture using MEA scrubbing: a flowsheet decomposition method. *Energy Convers. Manage.* **2005**, *46*, 475−487.
(94) Abu-Zahra, M. R.; Niederer, J. P.; Feron, P. H.; Versteeg, G. F. CO2 capture from power plants: Part II. A parametric study of the economical performance based on mono-ethanolamine. *Int. J. Greenhouse Gas Control* **2007**, *1*, 135−142.
(95) Rodríguez, N.; Mussati, S.; Scenna, N. Optimization of post-combustion CO2 process using DEA−MDEA mixtures. *Chem. Eng. Res. Des.* **2011**, *89*, 1763−1773.
(96) Mores, P.; Scenna, N.; Mussati, S. A rate based model of a packed column for CO_2 absorption using aqueous monoethanolamine solution. *Int. J. Greenhouse Gas Control* **2012**, *6*, 21−36.
(97) Hasan, M. M. F.; Baliban, R. C.; Elia, J. A.; Floudas, C. A. Modeling, Simulation, and Optimization of Postcombustion CO_2 Capture for Variable Feed Concentration and Flow Rate. 1. Chemical Absorption and Membrane Processes. *Ind. Eng. Chem. Res.* **2012**, *51*, 15642−15664.
(98) Feron, P.; Cousins, A.; Jiang, K.; Zhai, R.; Hla, S. S.; Thiruvenkatachari, R.; Burnard, K. Towards zero emissions from fossil fuel power stations. *Int. J. Greenhouse Gas Control* **2019**, *87*, 188−202.
(99) Bui, M.; Gunawan, I.; Verheyen, T.; Meuleman, E. Dynamic Operation of Liquid Absorbent-Based Post-Combustion CO_2 Capture Plants. *Absorption-Based Post-Combustion Capture of Carbon Dioxide*; Elsevier, 2016; pp 589−621.
(100) Mahasenan, N.; Brown, D. R. Beyond the Big Picture: Characterizaton of CO_2-Laden Streams and Implications for Capture Technologies. *Greenhouse Gas Control Technologies*; Elsevier, 2005; Vol. 7, pp 1817−1820.
(101) Mores, P.; Rodríguez, N.; Scenna, N.; Mussati, S. CO2 capture in power plants: Minimization of the investment and operating cost of the post-combustion process using MEA aqueous solution. *Int. J. Greenhouse Gas Control* **2012**, *10*, 148−163.
(102) Oh, S.-Y.; Kim, J.-K. Operational optimization for part-load performance of amine-based post-combustion CO2 capture processes. *Energy* **2018**, *146*, 57−66.
(103) Taylor, R.; Krishna, R. *Multicomponent Mass Transfer*; John Wiley & Sons, 1993; Vol. 2.
(104) Taylor, R.; Krishna, R.; Kooijman, H. Real-world modeling of distillation. *Chem. Eng. Prog.* **2003**, *99*, 28−39.
(105) Choi, J.; Cho, H.; Yun, S.; Jang, M.-G.; Oh, S.-Y.; Binns, M.; Kim, J.-K. Process design and optimization of MEA-based CO2 capture processes for non-power industries. *Energy* **2019**, *185*, 971−980.
(106) Asprion, N. True and Apparent Components in Reactive Systems. *Ind. Eng. Chem. Res.* **2004**, *43*, 8163−8167.
(107) Hilliard, M. D. A Predictive Thermodynamic Model for an Aqueous Blend of Potassium Carbonate, Piperazine, and Monoethanolamine for Carbon Dioxide Capture from Flue Gas. Ph.D. Thesis, The University of Texas at Austin, 2008.
(108) Morgan, J. C.; Chinen, A. S.; Omell, B.; Bhattacharyya, D.; Tong, C.; Miller, D. C. Thermodynamic modeling and uncertainty quantification of CO2-loaded aqueous MEA solutions. *Chem. Eng. Sci.* **2017**, *168*, 309−324.
(109) DeCoursey, W.; Thring, R. Effects of unequal diffusivities on enhancement factors for reversible and irreversible reaction. *Chem. Eng. Sci.* **1989**, *44*, 1715−1721.
(110) Morgan, J. C.; Bhattacharyya, D.; Tong, C.; Miller, D. C. Uncertainty quantification of property models: Methodology and its application to CO2-loaded aqueous MEA solutions. *AIChE J.* **2015**, *61*, 1822−1839.
(111) Agbonghae, E. O.; Hughes, K. J.; Ingham, D. B.; Ma, L.; Pourkashanian, M. A Semi-Empirical Model for Estimating the Heat Capacity of Aqueous Solutions of Alkanolamines for CO2 Capture. *Ind. Eng. Chem. Res.* **2014**, *53*, 8291−8301.
(112) Smith, J. M.; Van Ness, H. C.; Abbott, M. M. *Introduction to Chemical Engineering Thermodynamics*, 7th ed.; ACS Publications, 1950.
(113) Que, H.; Chen, C.-C. Thermodynamic Modeling of the NH3−CO2−H2O System with Electrolyte NRTL Model. *Ind. Eng. Chem. Res.* **2011**, *50*, 11406−11421.
(114) Kohl, A.; Riesenfeld, F. *Gas Purification*; Gulf Publishing Co. Book Division: Houston, 1985.
(115) Kohl, A. L.; Nielsen, R. *Gas Purification*; Gulf Professional Publishing, 1997.
(116) Jiru, Y.; Eimer, D. A.; Wenjuan, Y. Measurements and Correlation of Physical Solubility of Carbon Dioxide in (Monoethanolamine + Water) by a Modified Technique. *Ind. Eng. Chem. Res.* **2012**, *51*, 6958−6966.
(117) Ying, J.; Eimer, D. A. Measurements and Correlations of Diffusivities of Nitrous Oxide and Carbon Dioxide in Monoethanolamine + Water by Laminar Liquid Jet. *Ind. Eng. Chem. Res.* **2012**, *51*, 16517−16524.
(118) Sutherland, W. XXXVII. The viscosity of mixed gases. *London, Edinburgh Dublin Philos. Mag. J. Sci.* **1895**, *40*, 421−431.
(119) Wilke, C. R. A Viscosity Equation for Gas Mixtures. *J. Chem. Phys.* **1950**, *18*, 517−519.
(120) Reid, R. C.; Prausnitz, J. M.; Poling, B. E. *The Properties of Gases and Liquids*; U.S. Department of Energy, 1987.
(121) Li, C. Thermal conductivity of liquid mixtures. *AIChE J.* **1976**, *22*, 927−930.
(122) Seader, J.; Henly, E. *Seperation Process Principles*, 2nd ed.; John Wiley and Sons, Inc.: New York, 2006.
(123) Ying, J.; Eimer, D. A. Determination and measurements of mass transfer kinetics of CO2 in concentrated aqueous monoethanolamine solutions by a stirred cell. *Ind. Eng. Chem. Res.* **2013**, *52*, 2548−2559.
(124) Snijder, E. D.; te Riele, M. J.; Versteeg, G. F.; Van Swaaij, W. Diffusion coefficients of several aqueous alkanolamine solutions. *J. Chem. Eng. Data* **1993**, *38*, 475−480.
(125) Hoff, K. A.; Juliussen, O.; Falk-Pedersen, O.; Svendsen, H. F. Modeling and experimental study of carbon dioxide absorption in aqueous alkanolamine solutions using a membrane contactor. *Ind. Eng. Chem. Res.* **2004**, *43*, 4908−4921.
(126) Asprion, N. Surface tension models for aqueous amine blends. *Ind. Eng. Chem. Res.* **2005**, *44*, 7270−7278.
(127) Billet, R.; Schultes, M. Prediction of mass transfer columns with dumped and arranged packings: updated summary of the calculation method of Billet and Schultes. *Chem. Eng. Res. Des.* **1999**, *77*, 498−504.
(128) Tsai, R. E.; Seibert, A. F.; Eldridge, R. B.; Rochelle, G. T. A dimensionless model for predicting the mass-transfer area of structured packing. *AIChE J.* **2011**, *57*, 1173−1184.
(129) Kvamsdal, H. M.; Rochelle, G. T. Effects of the temperature bulge in CO2 absorption from flue gas by aqueous monoethanolamine. *Ind. Eng. Chem. Res.* **2008**, *47*, 867−875.
(130) Thimsen, D.; Maxson, A.; Smith, V.; Cents, T.; Falk-Pedersen, O.; Gorset, O.; Hamborg, E. S. Results from MEA testing at the CO2 Technology Centre Mongstad. Part I: Post-Combustion CO2 capture testing methodology. *Energy Procedia* **2014**, *63*, 5938−5958.
(131) Shah, M. I. In *CO_2 Capture from Rfcc Flue Gas with 30w% Mea at Technology Centre Mongstad, Process Optimization and Performance Comparison*, 14th Greenhouse Gas Control Technologies Conference Melbourne, 2018; pp 21−26.
(132) Turton, R.; Shaeiwitz, J. A.; Bhattacharyya, D.; Whiting, W. B. *Analysis, Synthesis, and Design of Chemical Processes*, 5th ed.; Prentice Hall: NJ, 2018; pp 221−223.

https://doi.org/10.1021/acs.iecr.0c05035
Ind. Eng. Chem. Res. XXXX, XXX, XXX−XXX